Available online at www.sciencedirect.com
ScienceDirect
Nuclear Physics B 957 (2020) 115082
NUCLEAR PHYSICS B
www.elsevier.com/locate/nuclphysb

Minimal extended seesaw and group symmetry realization of two-zero textures of neutrino mass matrices

Priyanka Kumar *, Mahadev Patgiri

Department of Physics, Cotton University, Guwahati, India

Received 31 December 2019; received in revised form 1 June 2020; accepted 3 June 2020
Available online 9 June 2020
Editor: Tommy Ohlsson

Abstract

We study the phenomenology of two-zero textures of $M_\nu^{4\times4}$ neutrino mass matrices in the minimal extended seesaw (MES) mechanism. $M_\nu^{4\times4}$ involves 3×3 Dirac neutrino mass matrix (M_D), 3×3 right-handed Majorana neutrino mass matrix M_R and 1×3 matrix M_S that couples the singlet field 'S' with the right-handed neutrinos. We consider the phenomenologically predictive cases (5+3) and (6+2) schemes for zero textures of M_D and M_R of 3×3 active sector of $M_\nu^{4\times4}$ along with admissible one or two-zero textures of M_S. Although there is a large number of combinations of M_D, M_R and M_S leading to the desired two-zero textures, S_3 group transformations between the different zero textures of M_D, M_R and M_S reduce them to a small number of basic combinations. In MES, $M_\nu^{4\times4}$ should be a matrix of rank 3, so we have 12 two-zero textures of neutrino mass matrices of rank 3 out of total 15 two-zero textures of neutrino mass matrices. In realization of the two-zero textures in (5+3) scheme we have obtained a number of correlations among the neutrino mass matrix elements m_{ij}, while none of the two-zero textures could be realized in the (6+2) scheme. The viability of each of the realizable textures is checked by plotting the scatter plots of their respective correlations under the current neutrino oscillation data. We have analysed the role played by the Dirac and Majorana CP phases for each of the textures. For constrained ranges of CP phases we also draw scatter plots for Jarlskog invariant (J_{CP}) and effective electron neutrino mass $|m_{\beta\beta}|$. In our study the viable textures are finally realized by Z_8 Abelian group symmetry by extending the Standard Model to include few scalar fields.

* Corresponding author.
E-mail addresses: prianca.kumar@gmail.com (P. Kumar), mahadevpatgiri@cottonuniversity.ac.in (M. Patgiri).

https://doi.org/10.1016/j.nuclphysb.2020.115082
0550-3213/

1. Introduction

The neutrino physics has been enriched with the knowledge and understanding of massive neutrinos by both theoretical and experimental endeavours for the last couple of decades, but this field of research is still striving for solutions of some anomalous results, for example, anomalies in short-baseline neutrino experiments. These results are either to be confirmed or to be ruled out in ongoing or upcoming experiments dedicated for the purpose. In literature, there are excellent review works of neutrino physics [1] in which this issue has also been addressed and the present status of sterile neutrino searches has been nicely reviewed in a recent paper [2]. The problem arises as follows: for the first time, an unexpected excess amount of $\bar{\nu_e}$-like events in the decay process $\mu^+ \to e^+ + \nu_e + \bar{\nu_\mu}$ was observed by the Liquid Scintillator Neutrino Detector (LSND) [3] in Fermi Laboratory, USA. In order to resolve the LSND anomaly, the Mini Booster Neutrino Experiment (MiniBooNE) was designed with the same oscillation frequency as that of the LSND experiment for detecting $\nu_\mu \to \nu_e$ and $\bar{\nu_\mu} \to \bar{\nu_e}$ signals [4]. MiniBooNE data have also corroborated the results of the LSND at the 4.7σ significance level.

The problem further deepens as about 15% deficit of the measured to predicted neutrino induced signal rates in the GALLEX [5] and SAGE [6] solar experiments was observed with 3σ significance level. This can be explained as $\nu_e \to \nu_e$ oscillations in $(3+1)$ scheme of active-sterile neutrino mixings with [7] $\Delta m^2_{41} \approx O(1)$ eV^2 and $sin^2\theta_{14} \approx O(10^{-2})$ to $O(10^{-1})$. Again, the reactor antineutrino anomaly stemmed from a 6% deficit of the observed $\bar{\nu_e}$ as compared to reactor antineutrino flux [8,9] of ^{235}U, ^{238}U, ^{239}Pu and ^{241}Pu with a significance of 3σ. But the recent analysis of Daya Bay data has rejected the hypothesis of a constant $\bar{\nu_e}$ flux as function of the ^{239}Pu fission fraction and also the hypothesis of a constant $\bar{\nu_e}$ energy spectrum, indicating that ^{235}U may be responsible for the reactor antineutrino anomaly [10]. There are a number of ongoing or upcoming short-baseline reactor antineutrino experiments viz., NEOS [11], DANSS [12], STEREO [13], PROSPECT [14], Neutrino-4 [15], SoLid [16] planned for achieving conclusive results about these anomalies.

For analysis of the data sets from short base-line neutrino experiments, the parameter space of three neutrino paradigm has no room as it has been already exhausted with the solar, atmospheric and reactor neutrino oscillation data. So to resolve such anomalies, phenomenologically a sterile neutrino state of eV mass scale which does not take part in Standard Model (SM) weak interaction but can mix with the active neutrinos was hypothesised in Ref. [17]. On the other hand, there arises a conflicting situation in cosmological context as the existence of a light thermalised sterile neutrino state is strongly disfavoured by the PLANCK data [18]. But in a number of interesting works [19–22] and references therein, it has been argued for re-look on a particle physics model of active-sterile neutrino mixing as well as a consistent cosmological model.

It is a pertinent question on the number of light sterile states if one considers the hypothesis of sterile neutrinos being the answer to the anomalous results. In literature, 3+1, 3+2, 3+3 (all having stable sterile states) [23], and 3+1+Decay (having unstable sterile state) [24] models of active-sterile states have been investigated in the light of global fits of data of various reactor, radio-chemical and accelerator based neutrino experiments. The conclusions of the papers are that there is internal inconsistency in 3+1 model if one separates the dataset of appearance experiments from the dataset of disappearance experiments. Then the natural choice is 3+2 model. But there is no compelling improvement of results in 3+2 model and so is the case of 3+3. The 3+2 model and beyond are not economical as there is a proliferation of oscillation parameters. The paper [25] concludes that the improvement of results in 3+2 model is a statistical effect for more number of oscillation parameters, whereas the paper [24] claims that there is a spectacular improvement in 3+1+decay model which relieves the internal tension in 3+1 model. As a first step, we are motivated to work with 3+1 models to address the issue of sterile neutrinos of ≈ 1 eV scale which will naturally be the simplest, minimal and more economical for extension of 3 active neutrino model.

The minimal extension of the existing 3-neutrino paradigm is the (3+1) scheme [26–29] to include one sterile neutrino and then one can calculate the probabilities of $\nu_\mu \rightarrow \nu_e$ and $\bar{\nu_\mu} \rightarrow \bar{\nu_e}$ to fix the LSND and MiniBooNE anomaly. The corresponding oscillation parameters are expected to be $\Delta m^2_{41} \approx O(1)$ eV^2 and $sin^2\theta_{14} \approx sin^2\theta_{24} \leqslant O(10^{-2})$ [2]. Similarly, the so-called gallium anomaly may be addressed as the consequence of $\nu_e \rightarrow \nu_e$ oscillations in (3+1) framework with values of parameters $\Delta m^2_{41} \approx O(1)$ eV^2 and $sin^2\theta_{14} \approx O(10^{-2})$ to $O(10^{-1})$ [7]. Again the reactor antineutrino anomaly also points toward the existence of an eV scale sterile state of neutrino with the active-sterile flavor mixing parameter $sin^2 2\theta_{14} \approx O(10^{-1})$ [30].

There may be some interesting phenomenological consequences of existence of one sterile neutrino species. For example, the disappearance oscillation probability of $\bar{\nu_e} \rightarrow \bar{\nu_e}$ may depend upon the possible values of θ_{14}, Δm^2_{41}, Δm^2_{42}. This will be concern for JUNO [31] experiment which is designed primarily for probing the neutrino mass hierarchy i.e., normal or inverted. Again the phenomenology of appearance neutrino/antineutrino oscillations such as $\nu_\mu \rightarrow \nu_e$ and $\bar{\nu_\mu} \rightarrow \bar{\nu_e}$ in the presence of one or more sterile neutrinos is very interesting which includes new CP-violating effects and neutral current associated matter effects [32–34]. Moreover, the presence of such new degrees of freedom will modify the effective mass term of the β decays and that of $0\nu 2\beta$ decays.

The origin of an eV scale sterile neutrino in (3+1) model has been studied in the framework of an extended version of the canonical type-I seesaw mechanism known as Minimal Extended Seesaw (MES) mechanism [17,35,36] whose formalism is briefly discussed in Section 2. The MES mechanism involves 3×3 Dirac neutrino mass matrix M_D, 3×3 right-handed Majorana neutrino mass matrix M_R and 1×3 row matrix M_S that couples the sterile state to the three right-handed neutrinos.

In literature one of the interesting approaches for investigating the phenomenology of neutrino mass models is the study of texture zeros of neutrino mass matrices. Initially the texture zero models were developed to calculate the Cabibbo angle of quark flavor mixing for both two-family [37–39] and three-family [40,41] scheme. The zeros or vanishing elements in the fermion mass matrices lead to reducing the number of free parameters of the complicated mass matrices and thereby establishing testable relations between the physical quantities: masses, mixing angles, and CP phases. Texture zeros of a given fermion mass matrix originates from proper choice of the flavor basis that has been chosen for the mass matrix [1]. More number of zeros in the mass matrices imply more restrictions on the free parameters thereby enhancing the predictivity of the models. Zeros in M_ν can be imposed directly by hand. From a more deeper theoretical front, zeros in M_ν can also be realized via type-I seesaw mechanism which has been considered to be more compatible for understanding the smallness of neutrino mass [42–46]. Thus one is tempted to study the texture zeros of M_D and M_R which are ingredients of the seesaw formula than the study of texture zeros of M_ν alone. This gives more insight into the problem. In addition, texture zeros of neutrino mass matrices indicate the underlying flavor symmetry. Zeros in arbitrary entries of the neutrino mass matrix M_ν can also be implemented via suitable Abelian flavor symmetry group Z_n with an extended scalar sector [47,48]. This provides a reasonable theoretical justification to phenomenological assumptions to texture zeros. Texture zeros of neutrino mass models in 3-active neutrino scenario, and (3+1) scheme with one sterile state, have been extensively studied in literature [49–63]. There is detailed study of phenomenologically allowed texture-zeros of neutrino mass matrix $M_\nu^{4\times4}$ in MES mechanism, assuming neutrinos to be Majorana fermions. With three active neutrinos, the light neutrino mass matrix $M_\nu^{3\times3}$ in the flavor basis can accommodate a maximum of two-zeros [64]. However, with one sterile neutrino i.e. (3+1) framework, one can have 1-4 possible zeros of $M_\nu^{4\times4}$ [61–63]. The MES neutrino mass matrix $M_\nu^{4\times4}$ is constructed with 3×3 Dirac neutrino mass matrix M_D, 3×3 right-handed Majorana neutrino mass matrix M_R and 1×3 mass matrix M_S. Fundamentally the texture-zeros of $M_\nu^{4\times4}$ are results of the texture-zeros of M_D, M_R and M_S via MES mechanism. In view of this, our primary focus in this work is to study the texture-zeros of these fermion mass matrices in the basis where the charged lepton mass matrix, M_l is diagonal and finally the viable zero textures shall be realized using Abelian flavor group symmetry Z_n by extending the scalar sector of the Standard Model (SM) of particle physics.

In the 3-neutrino paradigm, out of 15 possible two-zero textures, only 7 such textures remain viable within experimental constraints [64]. However, the compatibility conditions in the 3+1 framework are different. Out of 45 possible two-zero textures of $M_\nu^{4\times4}$, only 15 textures have been found to be compatible with experimental constraints [61]. Also, these 15 experimentally allowed textures of $M_\nu^{4\times4}$ are the same as the 15 possible two-zero textures of $M_\nu^{3\times3}$ in three active neutrino scenario. The texture zeros of $M_\nu^{3\times3}$ in type-I seesaw mechanism are the result for transmission from the zeros of M_D and M_R [43–46]. In the three neutrino paradigm, the author of Ref. [46] explored the zero textures for M_D and M_R for predictive cases, wherein the total number of zeros of M_D and M_R should be 8, irrespective of the number and/or position of zeros in the light neutrino mass matrix M_ν. Considering the predictive cases, the authors of the paper [65] studied in details one-zero textures of $M_\nu^{3\times3}$ in MES mechanism, while two-zero textures could not be realized. Although the two-zero textures with [61] or without [64] a sterile neutrino are phenomenologically allowed, but none of them in MES can be realised not only in predictive case [65] but also in other cases [66].

We are now motivated to revisit the two-zero textures in MES $M_\nu^{4\times4}$ obtained from the full neutrino mass matrix $M_\nu^{7\times7}$ subject to implementing the seesaw formula once. In this work, we adopt the conjecture that 3×3 active sector of this MES $M_\nu^{4\times4}$ in Eq. (3) also prefers the predictive scenario as they do in case of 3-active neutrino scenario. Phenomenology does not allow zero texture in sterile sector, i.e., no zero in the fourth row or column of $M_\nu^{4\times4}$ [61]. There are three possibilities in predictive scenario: (4+4) scheme, (5+3) scheme and (6+2) scheme, where the digits in the pairs represents the number of zeros of M_D and M_R respectively. Two-zero textures in $M_\nu^{4\times4}$ for (4+4) scheme within MES mechanism have already been studied in the paper [67]. In this paper we plan to explore the (5+3) and (6+2) schemes for realization of two-zero textures of MES $M_\nu^{4\times4}$ along with one and/or two-zero textures of M_S. It is to be noted that three-zero and four-zero texture of $M_\nu^{4\times4}$ can never be realized in the MES mechanism, as M_D and M_R should remain as non-singular in MES.

The MES 4×4 neutrino mass matrix is of rank 3, thus one of the mass eigenvalues should be massless and hence one has to consider one of the active neutrinos massless as vanishing sterile neutrino mass becomes trivial. So we have two mass patterns: normal hierarchy (NH) and inverted hierarchy (IH). 12 out of 15 allowed two-zero textures in $M_\nu^{4\times4}$ are of rank 3. We shall study all the 12 two-zero textures under the predictive scenario of (5+3) and (6+2) scheme. It is noted that none of the 12 two-zero textures can be realized within the (6+2) scheme. However, 9 out of 12 textures are found to be realizable within (5+3) scheme. We shall study all possible texture zeros of M_D and M_R and their S_3 transformations in the (5+3) scheme and check the consistency of the correlations of the textures by plotting scatter plots with the current neutrino oscillation data. We also study the Dirac and Majorana CP phases dependence of the coveted textures. In addition, we study the dependence of effective electron neutrino mass $|m_{\beta\beta}|$ on the lightest neutrino mass $m_{lightest}$ for the considered constrained range of Majorana CP phases for each texture. Also, we present scatter plots for Jarlskog invariant J_{CP} for each texture considering constrained range of Dirac CP phases.

The paper is organized as follows: In Section 2 we present a brief discussion on MES mechanism. Section 3 includes a brief review on the two-zero textures of $M_\nu^{3\times3}$. In its corresponding subsection 3.1, five-zero textures of M_D and three-zero textures of M_R along with zero textures of M_S is being presented. Also, S_3 permutation of fermion mass matrices under MES mechanism is presented in Sec. 3.1. In Section 4 we present the realization of the two-zero textures. In Section 5 we check the viability of the textures under recent neutrino oscillation data for both unconstrained and constrained CP phases. Also, scatter plots for $|m_{\beta\beta}|$ and J_{CP} for constrained CP phases are presented in this section. Symmetry realization of the viable textures are presented in Section 6. Finally, we conclude in Section 7 followed by the Appendix that contains the expressions for all ten elements m_{ij}, $(i, j = e, \mu, \tau, s)$ of the symmetric light neutrino mass matrix $M_\nu^{4\times4}$.

2. Minimal Extended Seesaw mechanism

The Minimal Extended Seesaw (MES) mechanism is an extension of the canonical type-I seesaw mechanism with an additional gauge singlet chiral field 'S' [17]. Thus, the fermion sector of the SM gets extended with four additional particles - the three right-handed neutrinos and one chiral field 'S'. Within this scenario, an eV scale sterile neutrino naturally appears without needing to insert any tiny Yukawa coupling or mass scales. The Lagrangian representing the mass term for neutrinos takes the form

$$-\mathcal{L}_m = \bar{\nu}_L M_D \nu_R + \bar{S}^c M_S \nu_R + \frac{1}{2}\bar{\nu}_R^c M_R \nu_R + h.c. \tag{1}$$

Here M_D, M_R are 3×3 Dirac and right-handed Majorana mass matrices respectively. As the extension is made with only one extra gauge singlet field 'S', therefore M_S which couples 'S' with the right-handed neutrinos ν_R's is a (1×3) row matrix. In the basis (ν_L, ν_R^c, S^c), the full neutrino mass matrix is a 7×7 matrix of the form:

$$M_\nu^{7\times7} = \begin{pmatrix} 0 & M_D & 0 \\ M_D^T & M_R & M_s^T \\ 0 & M_s & 0 \end{pmatrix}. \tag{2}$$

Considering the hierarchy $M_R \gg M_S > M_D$ and implementing type-I seesaw formula, the right-handed neutrinos get decoupled at low energy scales. The process of the block diagonalization of Eq. (2) leads to the effective neutrino mass matrix in the basis (ν_L, S^c) as

$$M_\nu^{4\times4} = -\begin{pmatrix} M_D M_R^{-1} M_D^T & M_D M_R^{-1} M_S^T \\ M_S (M_R^{-1})^T M_D^T & M_S M_R^{-1} M_S^T \end{pmatrix}. \tag{3}$$

The square matrix in Eq. (3) contains four light eigenstates corresponding to three active neutrinos and one sterile neutrino [35]. However, the determinant of the mass matrix $M_\nu^{4\times4}$ is zero with the condition of M_D and M_R being non-singular. Thus the mass matrix $M_\nu^{4\times4}$ is a matrix of rank 3. This implies that at least one of the active neutrino mass states remains as massless, while the sterile neutrino mass is

$$m_s \simeq -M_S M_R^{-1} M_S^T. \tag{4}$$

In Ref. [17] the authors explained that similar to type-I seesaw formula, in MES also M_D and M_R can assume masses around the electroweak scale ≈ 100 GeV and the grand unification scale $\approx 10^{14}$ GeV respectively. Furthermore, there is no bare mass term for the gauge singlet chiral field, S, being involved in M_S term of the Lagrangian in Eq. (1) which originates from certain Yukawa interactions with right-handed neutrinos and a SM singlet scalar. Hence the mass scale of M_S is not constrained. For an illustration, assuming $M_D \approx 10^2$ GeV, $M_S \approx 5 \times 10^2$ GeV and $M_R \approx 2 \times 10^{14}$ GeV, one gets $m_\nu \approx 0.05$ eV and a sterile neutrino of mass $m_s \approx 1.3$ eV.

Assuming the charged lepton mass matrix to be diagonal, in the flavor basis the 4×4 Majorana neutrino mass matrix can be expressed as

$$M_\nu^{4\times4} = V M_\nu^{diag} V^T = \begin{pmatrix} m_{ee} & m_{e\mu} & m_{e\tau} & m_{es} \\ m_{e\mu} & m_{\mu\mu} & m_{\mu\tau} & m_{\mu s} \\ m_{e\tau} & m_{\mu\tau} & m_{\tau\tau} & m_{\tau s} \\ m_{es} & m_{\mu s} & m_{\tau s} & m_{ss} \end{pmatrix}, \tag{5}$$

where V corresponds to the 4×4 PMNS lepton mixing matrix and $M_\nu^{diag} = diag(m_1, m_2, m_3, m_4)$. The mass matrix elements of Eq. (5) are presented in the appendix section.

Considering the parametrization of the 4×4 PMNS lepton mixing matrix as [68]

$$V = UP, \tag{6}$$

where

$$U = (R_{34}\tilde{R}_{24}\tilde{R}_{14})(R_{23}\tilde{R}_{13})R_{12}, \tag{7}$$

$$P = diag(1, e^{-i\alpha/2}, e^{-i(\beta/2-\delta_{13})}, e^{-i(\gamma/2-\delta_{14})}). \tag{8}$$

Here α, β, γ are the Majorana phases and $R_{ij}/\tilde{R}_{ij}$ are the rotation matrices in the ij flavor space with $\delta_{13}, \delta_{14}, \delta_{24}$ as the Dirac CP phases, e.g.,

$$R_{34} = \begin{pmatrix} 1 & 0 & 0 & 0 \\ 0 & 1 & 0 & 0 \\ 0 & 0 & c_{34} & s_{34} \\ 0 & 0 & -s_{34} & c_{34} \end{pmatrix}, \quad \tilde{R}_{24} = \begin{pmatrix} 1 & 0 & 0 & 0 \\ 0 & c_{24} & 0 & s_{24}e^{-i\delta_{24}} \\ 0 & 0 & 1 & 0 \\ 0 & -s_{24}e^{i\delta_{24}} & 0 & c_{24} \end{pmatrix}. \tag{9}$$

$c_{ij} = \cos\theta_{ij}$, $s_{ij} = \sin\theta_{ij}$.

The current experimental data on the oscillation parameters for 3-neutrino as well as for (3+1)-picture are given in Table 1.

3. Two-zero textures of $M_\nu^{4\times4}$

In MES $M_\nu^{4\times4}$ matrices are required to be of rank 3 as one of the mass eigenvalue value of active neutrinos is to vanish. There are 12 possible two-zero textures of $M_\nu^{4\times4}$ which are of rank 3 presented in Table 2. In this work we have conjectured that the predictive case is the a priori condition for the total number of zeros of M_D and M_R being 8 in the active sector of $M_\nu^{4\times4}$ as they follow in the type-I seesaw without sterile neutrino. There are three possibilities (a) 4+4, (b) 5+3 and (c) 6+2 for predictive scenario. The (4+4) predictive scheme was studied in the paper [67]. Now we are motivated to study (5+3) and (6+2) schemes of predictive cases. In the paper [61] authors found the following: (i) the textures A_1 and A_2 belong to class A, which allow only the normal hierarchical mass patterns, (ii) the textures D_1, D_2 of class D allow both NH and IH mass orderings, (iii) the textures B_3, B_4 of class B and F_1, F_2, F_3 of class F favours all the three

Table 1
Best fit and 3σ values of active ν oscillation parameters [69] and the current constraints on sterile neutrino parameters [70–72]. Here R_ν is the solar to atmospheric mass squared difference ratio.

Parameter	Best fit	3σ range
$\Delta m^2_{21}[10^{-5}\ \text{eV}^2]$	7.37	6.93-7.97
$\Delta m^2_{31}[10^{-3}\ \text{eV}^2]$ (NH)	2.50	2.37-2.63
$\Delta m^2_{31}[10^{-3}\ \text{eV}^2]$ (IH)	2.46	2.33-2.60
$\sin^2\theta_{12}/10^{-1}$	2.97	2.50-3.54
$\sin^2\theta_{13}/10^{-2}$ (NH)	2.14	1.85-2.46
$\sin^2\theta_{13}/10^{-2}$ (IH)	2.18	1.86-2.48
$\sin^2\theta_{23}/10^{-1}$ (NH)	4.37	3.79-6.16
$\sin^2\theta_{23}/10^{-1}$ (IH)	5.69	3.83-6.37
δ_{13}/π (NH)	1.35	0-2
δ_{13}/π (IH)	1.32	0-2
R_ν (NH)	0.0295	0.0263-0.0336
R_ν (IH)	0.0299	0.0266-0.0342
$\Delta m^2_{LSND}(\Delta m^2_{41}$ or $\Delta m^2_{43})$ eV^2	1.63	0.87-2.04
$\lvert V_{e4}\rvert^2$	0.027	0.012-0.047
$\lvert V_{\mu 4}\rvert^2$	0.013	0.005-0.03
$\lvert V_{\tau 4}\rvert^2$	–	< 0.16

Table 2
Viable two-zero textures [61] of rank 3. Here 'X' indicates the elements with non-zero entries.

A_1	A_2	B_3	B_4
$\begin{pmatrix} 0 & 0 & X & X \\ 0 & X & X & X \\ X & X & X & X \\ X & X & X & X \end{pmatrix}$	$\begin{pmatrix} 0 & X & 0 & X \\ X & X & X & X \\ 0 & X & X & X \\ X & X & X & X \end{pmatrix}$	$\begin{pmatrix} X & 0 & X & X \\ 0 & 0 & X & X \\ X & X & X & X \\ X & X & X & X \end{pmatrix}$	$\begin{pmatrix} X & X & 0 & X \\ X & X & X & X \\ 0 & X & 0 & X \\ X & X & X & X \end{pmatrix}$
C	D_1	D_2	E_1
$\begin{pmatrix} X & X & X & X \\ X & 0 & X & X \\ X & X & 0 & X \\ X & X & X & X \end{pmatrix}$	$\begin{pmatrix} X & X & X & X \\ X & 0 & 0 & X \\ X & 0 & X & X \\ X & X & X & X \end{pmatrix}$	$\begin{pmatrix} X & X & X & X \\ X & X & 0 & X \\ X & 0 & 0 & X \\ X & X & X & X \end{pmatrix}$	$\begin{pmatrix} 0 & X & X & X \\ X & 0 & X & X \\ X & X & X & X \\ X & X & X & X \end{pmatrix}$
E_2	F_1	F_2	F_3
$\begin{pmatrix} 0 & X & X & X \\ X & X & X & X \\ X & X & 0 & X \\ X & X & X & X \end{pmatrix}$	$\begin{pmatrix} X & 0 & 0 & X \\ 0 & X & X & X \\ 0 & X & X & X \\ X & X & X & X \end{pmatrix}$	$\begin{pmatrix} X & 0 & X & X \\ 0 & X & 0 & X \\ X & 0 & X & X \\ X & X & X & X \end{pmatrix}$	$\begin{pmatrix} X & X & 0 & X \\ X & X & 0 & X \\ 0 & 0 & X & X \\ X & X & X & X \end{pmatrix}$

mass patterns: normal hierarchy (NH), inverted hierarchy (IH) and quasi degenerate (QD). As one of the mass eigenvalues of the matrix $M_\nu^{4\times 4}$ in MES is massless, so the NH and IH mass patterns of the textures are allowed in MES but the QD textures are not allowed. In advance we note from our work that the textures C, E_1, E_2 can not be realized under (5+3) scheme and also no one of the textures can be realized under (6+2) scheme in the context of MES mechanism.

Also, $P_{\mu\tau}$ symmetry [61] exists between the textures $A_1 - A_2$; $B_3 - B_4$; $D_1 - D_2$ and $F_2 - F_3$ according to Eq. (10). However, such a symmetry does not exist for the texture F_1.

$$B_4 = P^T_{\mu\tau} B_3 P_{\mu\tau}, \tag{10}$$

where

$$P_{\mu\tau} = \begin{pmatrix} 1 & 0 & 0 & 0 \\ 0 & 0 & 1 & 0 \\ 0 & 1 & 0 & 0 \\ 0 & 0 & 0 & 1 \end{pmatrix}. \quad (11)$$

3.1. (5+3) scheme and S_3 permutation group

There are a number of combinations of M_D, M_R and M_S for which the mass matrices $M_\nu^{4\times4}$ in Eq. (3) remain invariant under S_3 transformations that lead to the same correlations. These transformations reduce the voluminous work of dealing with a large number of possible combinations of M_D, M_R and M_S under the (5+3) scheme to only a few basic combinations. The following S_3 transformations of M_D, M_R and M_S[1] keep $M_\nu^{4\times4}$ invariant:

$$M_D \to M_D Z, \quad M_R \to Z^T M_R Z, \quad M_S \to M_S Z \quad (12)$$

Here Z represents the six elements of the S_3 permutation group

$$Z \in S_3 = (A, A^2, B, AB, BA, ABA) \quad (13)$$

where

$$A = \begin{pmatrix} 0 & 1 & 0 \\ 1 & 0 & 0 \\ 0 & 0 & 1 \end{pmatrix}, \quad B = \begin{pmatrix} 0 & 0 & 1 \\ 0 & 1 & 0 \\ 1 & 0 & 0 \end{pmatrix} \quad (14)$$

<u>3-zero textures of M_R</u>:

The right-handed Majorana mass matrix M_R is symmetric with six independent entries and so we have ${}^6C_3 = 20$ possible 3-zero textures, out of which only 14 are non-singular (Table 3). According to Eq. (12) S_3 group permutations enable us to work with only four basic 3-zero textures of M_R: $M_R^{(1)}$, $M_R^{(7)}$, $M_R^{(9)}$ and $M_R^{(10)}$. However, it has been observed that all the elements of the inverse of $M_R^{(1)}$ are non-zero and as a result, no zero in $M_\nu^{4\times4}$ can be generated via MES mechanism. So $M_R^{(1)}$ is redundant. Thus, only 13 three-zero textures of M_R shall be considered for investigation and three basic textures: $M_R^{(7)}$, $M_R^{(9)}$ and $M_R^{(10)}$.

$$M_R^{(7)} = \begin{pmatrix} A & 0 & 0 \\ 0 & D & 0 \\ 0 & 0 & F \end{pmatrix}, M_R^{(9)} = \begin{pmatrix} A & B & 0 \\ B & 0 & E \\ 0 & E & 0 \end{pmatrix}, M_R^{(10)} = \begin{pmatrix} A & B & 0 \\ B & 0 & 0 \\ 0 & 0 & F \end{pmatrix}. \quad (15)$$

<u>5-zero textures of M_D</u>:

As the Dirac neutrino mass matrices are non-symmetric with all 9 elements being independent, there might be ${}^9C_5 = 126$ possible 5-zero textures. However, as the MES mechanism demands M_D to be non-singular, 90 such textures of M_D which have either row zero, column zero or block zero are not useful for being singular. The remaining 36 non-singular textures are

[1] M_ν, M_R and $M_S^T M_S$ are symmetric and hence they entail permutations of both rows and columns.

Table 3
All possible non-singular three-zero textures of M_R.

$M_R^{(1)}$	$M_R^{(2)}$	$M_R^{(3)}$	$M_R^{(4)}$
$\begin{pmatrix} 0 & B & C \\ B & 0 & E \\ C & E & 0 \end{pmatrix}$	$\begin{pmatrix} 0 & 0 & C \\ 0 & D & E \\ C & E & 0 \end{pmatrix}$	$\begin{pmatrix} 0 & B & 0 \\ B & 0 & E \\ 0 & E & F \end{pmatrix}$	$\begin{pmatrix} 0 & 0 & C \\ 0 & D & 0 \\ C & 0 & F \end{pmatrix}$
$M_R^{(5)}$	$M_R^{(6)}$	$M_R^{(7)}$	$M_R^{(8)}$
$\begin{pmatrix} A & 0 & C \\ 0 & 0 & E \\ C & E & 0 \end{pmatrix}$	$\begin{pmatrix} A & 0 & 0 \\ 0 & 0 & E \\ 0 & E & F \end{pmatrix}$	$\begin{pmatrix} A & 0 & 0 \\ 0 & D & 0 \\ 0 & 0 & F \end{pmatrix}$	$\begin{pmatrix} A & 0 & 0 \\ 0 & D & E \\ 0 & E & 0 \end{pmatrix}$
$M_R^{(9)}$	$M_R^{(10)}$	$M_R^{(11)}$	$M_R^{(12)}$
$\begin{pmatrix} A & B & 0 \\ B & 0 & E \\ 0 & E & 0 \end{pmatrix}$	$\begin{pmatrix} A & B & 0 \\ B & 0 & 0 \\ 0 & 0 & F \end{pmatrix}$	$\begin{pmatrix} 0 & B & C \\ B & 0 & 0 \\ C & 0 & F \end{pmatrix}$	$\begin{pmatrix} 0 & B & C \\ B & D & 0 \\ C & 0 & 0 \end{pmatrix}$
$M_R^{(13)}$	$M_R^{(14)}$	–	–
$\begin{pmatrix} 0 & B & 0 \\ B & D & 0 \\ 0 & 0 & F \end{pmatrix}$	$\begin{pmatrix} A & 0 & C \\ 0 & D & 0 \\ C & 0 & 0 \end{pmatrix}$	–	–

viable. Again we find that 26 textures of M_D (Table 4) out of aforesaid 36 textures play the role in the basic combinations with M_R in Eq. (15) and M_S (Eq. (16), (17)) to reproduce the desired two-zero textures of $M_\nu^{4\times4}$. All other combinations can be obtained via S_3 transformations according to Eq. (12).

Zero textures of M_S:

The 1×3 row matrix $M_S = \begin{pmatrix} s_1 & s_2 & s_3 \end{pmatrix}$ can have two possible zero textures:

(1) One-zero textures:

$$M_S^{(1)} = \begin{pmatrix} 0 & s_2 & s_3 \end{pmatrix}, \quad M_S^{(2)} = \begin{pmatrix} s_1 & 0 & s_3 \end{pmatrix}, \quad M_S^{(3)} = \begin{pmatrix} s_1 & s_2 & 0 \end{pmatrix}. \tag{16}$$

(2) Two-zero textures:

$$M_S^{(4)} = \begin{pmatrix} s_1 & 0 & 0 \end{pmatrix}, \quad M_S^{(5)} = \begin{pmatrix} 0 & s_2 & 0 \end{pmatrix}, \quad M_S^{(6)} = \begin{pmatrix} 0 & 0 & s_3 \end{pmatrix}. \tag{17}$$

4. Realization of two-zero textures

We have 36 five-zero textures of M_D, 13 three-zero textures of M_R and 6 one and two-zero textures of M_S under (5+3) scheme mentioned in the previous section to realize the two-zero textures of $M_\nu^{4\times4}$ in MES. Although there exist 2808 number of possible choices for the combinations of M_D, M_R and M_S in the framework of MES, but 252 number of possible combinations are effective for realization of our desired two-zero textures of $M_\nu^{4\times4}$. Again the complexity of the texture study of these 252 combinations can further be reduced by S_3 transformations to only 42 basic combinations for each of which there are five S_3 transformations. The zeros of M_D, M_R and M_S propagate to $M_\nu^{4\times4}$ through MES formula in Eq. (3) which acquires a form of two-zero texture. In this process we also obtain the correlations among some of the matrix elements m_{ij}

Table 4
5-zero textures of M_D required in basic combinations.

$M_D^{(1)}$	$M_D^{(2)}$	$M_D^{(3)}$	$M_D^{(4)}$
$\begin{pmatrix} a & 0 & 0 \\ 0 & 0 & f \\ 0 & h & l \end{pmatrix}$	$\begin{pmatrix} 0 & b & 0 \\ d & 0 & 0 \\ g & 0 & l \end{pmatrix}$	$\begin{pmatrix} 0 & b & 0 \\ d & e & 0 \\ 0 & 0 & l \end{pmatrix}$	$\begin{pmatrix} 0 & b & 0 \\ d & 0 & 0 \\ 0 & h & l \end{pmatrix}$
$M_D^{(5)}$	$M_D^{(6)}$	$M_D^{(7)}$	$M_D^{(8)}$
$\begin{pmatrix} a & 0 & 0 \\ d & 0 & f \\ 0 & h & 0 \end{pmatrix}$	$\begin{pmatrix} a & 0 & 0 \\ 0 & e & f \\ 0 & 0 & l \end{pmatrix}$	$\begin{pmatrix} a & 0 & 0 \\ 0 & e & 0 \\ g & 0 & h \end{pmatrix}$	$\begin{pmatrix} 0 & b & 0 \\ d & 0 & f \\ g & 0 & 0 \end{pmatrix}$
$M_D^{(9)}$	$M_D^{(10)}$	$M_D^{(11)}$	$M_D^{(12)}$
$\begin{pmatrix} 0 & b & 0 \\ 0 & e & f \\ g & 0 & 0 \end{pmatrix}$	$\begin{pmatrix} 0 & b & 0 \\ 0 & 0 & f \\ g & h & 0 \end{pmatrix}$	$\begin{pmatrix} a & b & 0 \\ 0 & e & 0 \\ 0 & 0 & l \end{pmatrix}$	$\begin{pmatrix} a & 0 & c \\ d & 0 & 0 \\ 0 & h & 0 \end{pmatrix}$
$M_D^{(13)}$	$M_D^{(14)}$	$M_D^{(15)}$	$M_D^{(16)}$
$\begin{pmatrix} a & 0 & 0 \\ 0 & e & 0 \\ 0 & h & l \end{pmatrix}$	$\begin{pmatrix} 0 & 0 & c \\ d & 0 & 0 \\ 0 & h & l \end{pmatrix}$	$\begin{pmatrix} a & b & 0 \\ 0 & 0 & f \\ 0 & h & 0 \end{pmatrix}$	$\begin{pmatrix} a & 0 & c \\ 0 & e & 0 \\ g & 0 & 0 \end{pmatrix}$
$M_D^{(17)}$	$M_D^{(18)}$	$M_D^{(19)}$	$M_D^{(20)}$
$\begin{pmatrix} a & 0 & 0 \\ 0 & e & f \\ 0 & h & 0 \end{pmatrix}$	$\begin{pmatrix} 0 & 0 & c \\ 0 & e & f \\ g & 0 & 0 \end{pmatrix}$	$\begin{pmatrix} 0 & b & c \\ d & 0 & 0 \\ 0 & 0 & l \end{pmatrix}$	$\begin{pmatrix} 0 & b & c \\ 0 & e & 0 \\ g & 0 & 0 \end{pmatrix}$
$M_D^{(21)}$	$M_D^{(22)}$	$M_D^{(23)}$	$M_D^{(24)}$
$\begin{pmatrix} 0 & 0 & c \\ 0 & e & 0 \\ g & h & 0 \end{pmatrix}$	$\begin{pmatrix} 0 & b & c \\ d & 0 & 0 \\ 0 & h & 0 \end{pmatrix}$	$\begin{pmatrix} 0 & b & c \\ 0 & 0 & f \\ g & 0 & 0 \end{pmatrix}$	$\begin{pmatrix} 0 & 0 & c \\ d & e & 0 \\ 0 & h & 0 \end{pmatrix}$
$M_D^{(25)}$	$M_D^{(26)}$	–	–
$\begin{pmatrix} a & b & 0 \\ d & 0 & 0 \\ 0 & 0 & l \end{pmatrix}$	$\begin{pmatrix} a & 0 & 0 \\ d & e & 0 \\ 0 & 0 & l \end{pmatrix}$	–	–

with $i, j = e, \mu, \tau, s$ of $M_\nu^{4\times4}$ as results of the functional relations among the parameters of M_D, M_R and M_S. Again the question of viability of a two-zero texture is addressed by the consistency check of these correlations under the current neutrino data. This analysis shall follow in the next section. Now we present three representative cases out of 42 basic combinations for understanding of the problem:

Case I: The following basic combination of

$$M_R = M_R^{(9)}, \qquad M_D = M_D^{(11)}, \qquad M_S = M_S^{(6)}, \tag{18}$$

in Eq. (15), Table 4 and Eq. (17) respectively used in Eq. (3) leads to the form of $M_\nu^{4\times4}$ as

$$M_\nu^{4\times4} = \begin{pmatrix} \frac{a^2}{A} & 0 & \frac{(bA-aB)l}{AE} & \frac{(bA-aB)s_3}{AE} \\ 0 & 0 & \frac{el}{E} & \frac{es_3}{E} \\ \frac{(bA-aB)l}{AE} & \frac{el}{E} & \frac{l^2B^2}{AE^2} & \frac{ls_3B^2}{AE^2} \\ \frac{(bA-aB)s_3}{AE} & \frac{es_3}{E} & \frac{ls_3B^2}{AE^2} & \frac{s_3^2B^2}{AE^2} \end{pmatrix}. \tag{19}$$

Table 5
S_3 symmetric textures of the basic combination in Eq. (18).

Case	M_D	M_R	M_S
(a)	$\begin{pmatrix} a & b & 0 \\ d & 0 & 0 \\ 0 & 0 & l \end{pmatrix}$	$M_R^{(12)}$	$M_S^{(6)}$
(b)	$\begin{pmatrix} 0 & b & c \\ 0 & e & 0 \\ g & 0 & 0 \end{pmatrix}$	$M_R^{(3)}$	$M_S^{(4)}$
(c)	$\begin{pmatrix} 0 & b & c \\ 0 & 0 & f \\ g & 0 & 0 \end{pmatrix}$	$M_R^{(2)}$	$M_S^{(5)}$
(d)	$\begin{pmatrix} a & 0 & c \\ d & 0 & 0 \\ 0 & h & 0 \end{pmatrix}$	$M_R^{(11)}$	$M_S^{(4)}$
(e)	$\begin{pmatrix} a & 0 & c \\ 0 & 0 & f \\ 0 & h & 0 \end{pmatrix}$	$M_R^{(5)}$	$M_S^{(4)}$

This is the texture B_3 in Table 2 and reproduces the following correlation

$$\frac{m_{e\tau}}{m_{es}} = \frac{m_{\mu\tau}}{m_{\mu s}} = \frac{m_{\tau\tau}}{m_{\tau s}} = \frac{m_{\tau s}}{m_{ss}} = \sqrt{\frac{m_{\tau\tau}}{m_{ss}}} \tag{20}$$

According to Eq. (12) S_3 transformations of the basic combination in Eq. (18) give a number of cases which generate textures B_3 with the same correlations as in Eq. (20). These are presented in Table 5.

<u>Case II</u>: Another basic combination of

$$M_R = M_R^{(9)}, \qquad M_D = M_D^{(21)}, \qquad M_S = M_S^{(6)}, \tag{21}$$

in Eq. (15), Table 4 and Eq. (17) respectively applied in Eq. (3) produces the following $M_\nu^{4\times4}$

$$M_\nu^{4\times4} = \begin{pmatrix} \frac{c^2B^2}{AE^2} & \frac{ce}{E} & \frac{(hA-gB)c}{AE} & \frac{cs_3AE^2}{B^2} \\ \frac{ce}{E} & 0 & 0 & \frac{es_3}{E} \\ \frac{(hA-gB)c}{AE} & 0 & \frac{g^2}{A} & \frac{(hA-gB)s_3}{AE} \\ \frac{cs_3AE^2}{B^2} & \frac{es_3}{E} & \frac{(hA-gB)s_3}{AE} & \frac{s_3^2B^2}{AE^2} \end{pmatrix}. \tag{22}$$

This is of the texture D_1 in Table 2 that leads to the following correlation

$$\frac{m_{ee}}{m_{es}} = \frac{m_{es}}{m_{ss}} = \frac{m_{e\tau}}{m_{\tau s}} = \frac{m_{e\mu}}{m_{\mu s}} = \sqrt{\frac{m_{ee}}{m_{ss}}} \tag{23}$$

In this case also there exist another five combinations of M_D, M_R, M_S which are S_3 symmetric to Eq. (21) giving the same correlation as in Eq. (23) (Table 6).

<u>Case III</u>: The basic combination of

$$M_R^{(9)}, M_D^{(5)}, M_S^{(6)} \tag{24}$$

Table 6
S_3 symmetric textures of the basic combination in Eq. (21).

Case	M_D	M_R	M_S
(a)	$\begin{pmatrix} 0 & 0 & c \\ d & 0 & 0 \\ g & h & 0 \end{pmatrix}$	$M_R^{(12)}$	$M_S^{(6)}$
(b)	$\begin{pmatrix} a & 0 & 0 \\ 0 & e & 0 \\ 0 & h & l \end{pmatrix}$	$M_R^{(3)}$	$M_S^{(4)}$
(c)	$\begin{pmatrix} a & 0 & 0 \\ 0 & 0 & f \\ 0 & h & l \end{pmatrix}$	$M_R^{(2)}$	$M_S^{(5)}$
(d)	$\begin{pmatrix} 0 & b & 0 \\ d & 0 & 0 \\ g & 0 & l \end{pmatrix}$	$M_R^{(11)}$	$M_S^{(4)}$
(e)	$\begin{pmatrix} 0 & b & 0 \\ 0 & 0 & f \\ g & 0 & l \end{pmatrix}$	$M_R^{(5)}$	$M_S^{(4)}$

Table 7
S_3 symmetric textures of the basic combination in Eq. (24).

Case	M_D	M_R	M_S
(a)	$\begin{pmatrix} 0 & b & 0 \\ 0 & e & f \\ h & 0 & 0 \end{pmatrix}$	$M_R^{(12)}$	$M_S^{(6)}$
(b)	$\begin{pmatrix} 0 & 0 & c \\ d & 0 & f \\ 0 & h & 0 \end{pmatrix}$	$M_R^{(3)}$	$M_S^{(4)}$
(c)	$\begin{pmatrix} 0 & b & 0 \\ d & e & 0 \\ 0 & 0 & l \end{pmatrix}$	$M_R^{(2)}$	$M_S^{(5)}$
(d)	$\begin{pmatrix} 0 & 0 & c \\ 0 & e & f \\ g & 0 & 0 \end{pmatrix}$	$M_R^{(11)}$	$M_S^{(4)}$
(e)	$\begin{pmatrix} a & 0 & 0 \\ d & e & 0 \\ 0 & 0 & h \end{pmatrix}$	$M_R^{(5)}$	$M_S^{(4)}$

in Eq. (15), Table 4 and Eq. (17) respectively used in Eq. (3) leads to the texture B_4 and it reproduces two correlations:

$$\frac{m_{e\mu}}{m_{\mu s}} = \frac{m_{ee}}{m_{es}} \tag{25}$$

$$m_{ee}m_{ss} = m_{es}^2 \tag{26}$$

However, there exist another five combinations (Table 7) which are S_3 symmetric to Eq. (24) giving the same correlations as in Eq. (25) and (26).

Table 8
Basic combination required for realization of the allowed two-zero textures under (5+3) scheme and their respective correlations.

Texture	M_D, M_R, M_S	Correlations
$A_1(i)$	(1), (10), (1)	$m_{es}(m_{\tau s}m_{\mu\mu}-m_{\mu\tau}m_{\mu s})=m_{e\tau}(m_{ss}m_{\mu\mu}-m_{\mu s}^2)$
(ii)	(2), (9), (6)	$(a)\quad \frac{m_{\mu\tau}}{m_{\mu\mu}}=\frac{m_{\tau s}}{m_{\mu s}},\quad (b)\quad m_{\mu\mu}m_{ss}=m_{\mu s}^2$
(iii)	(3), (9), (6)	$\frac{m_{e\tau}}{m_{es}}=\frac{m_{\mu\tau}}{m_{\mu s}}=\frac{m_{\tau\tau}}{m_{\tau s}}=\frac{m_{\tau s}}{m_{ss}}=\sqrt{\frac{m_{\tau\tau}}{m_{ss}}}$
(iv)	(4), (9), (6)	$(a)\quad \frac{m_{e\tau}}{m_{es}}=\frac{m_{\mu\tau}}{m_{\mu s}},\quad (b)\quad m_{\mu\mu}m_{ss}=m_{\mu s}^2$
(v)	(5), (10), (5)	$\frac{m_{e\tau}}{m_{es}}=\frac{m_{\mu\tau}}{m_{\mu s}}=\frac{m_{\tau\tau}}{m_{\tau s}}=\frac{m_{\tau s}}{m_{ss}}=\sqrt{\frac{m_{\tau\tau}}{m_{ss}}}$
$A_2(i)$	(6), (10), (1)	$m_{es}(m_{\mu s}m_{\tau\tau}-m_{\mu\tau}m_{\tau s})=m_{e\mu}(m_{ss}m_{\tau\tau}-m_{\tau s}^2)$
(ii)	(8), (9), (6)	$(a)\quad \frac{m_{\mu\tau}}{m_{\tau\tau}}=\frac{m_{\mu s}}{m_{\tau s}},\quad (b)\quad m_{\tau\tau}m_{ss}=m_{\tau s}^2$
(iii)	(7), (10), (5)	$\frac{m_{e\mu}}{m_{es}}=\frac{m_{\mu\tau}}{m_{\tau s}}=\frac{m_{\mu\mu}}{m_{\mu s}}=\frac{m_{\mu s}}{m_{ss}}=\sqrt{\frac{m_{\mu\mu}}{m_{ss}}}$
(iv)	(9), (9), (6)	$(a)\quad \frac{m_{e\mu}}{m_{es}}=\frac{m_{\mu\tau}}{m_{\tau s}},\quad (b)\quad m_{\tau\tau}m_{ss}=m_{\tau s}^2$
(v)	(10), (9), (6)	$\frac{m_{e\mu}}{m_{es}}=\frac{m_{\mu\tau}}{m_{\tau s}}=\frac{m_{\mu\mu}}{m_{\mu s}}=\frac{m_{\mu s}}{m_{ss}}=\sqrt{\frac{m_{\mu\mu}}{m_{ss}}}$
$B_3(i)$	(11), (9), (6)	$\frac{m_{e\tau}}{m_{es}}=\frac{m_{\mu\tau}}{m_{\mu s}}=\frac{m_{\tau\tau}}{m_{\tau s}}=\frac{m_{\tau s}}{m_{ss}}=\sqrt{\frac{m_{\tau\tau}}{m_{ss}}}$
(ii)	(12), (10), (5)	$\frac{m_{e\tau}}{m_{es}}=\frac{m_{\mu\tau}}{m_{\mu s}}=\frac{m_{\tau\tau}}{m_{\tau s}}=\frac{m_{\tau s}}{m_{ss}}=\sqrt{\frac{m_{\tau\tau}}{m_{ss}}}$
(iii)	(7), (9), (6)	$(a)\quad \frac{m_{e\tau}}{m_{\tau s}}=\frac{m_{ee}}{m_{es}},\quad (b)\quad m_{ee}m_{ss}=m_{es}^2$
(iv)	(13), (9), (6)	$(a)\quad \frac{m_{e\tau}}{m_{es}}=\frac{m_{\mu\tau}}{m_{\mu s}},\quad (b)\quad m_{ee}m_{ss}=m_{es}^2$
(v)	(14), (10), (1)	$m_{ee}(m_{\tau\tau}m_{\mu s}-m_{\mu\tau}m_{\tau s})=m_{e\tau}(m_{e\tau}m_{\mu s}-m_{es}m_{\mu\tau})$
$B_4(i)$	(15), (9), (6)	$\frac{m_{e\mu}}{m_{es}}=\frac{m_{\mu\tau}}{m_{\tau s}}=\frac{m_{\mu\mu}}{m_{\mu s}}=\frac{m_{\mu s}}{m_{ss}}=\sqrt{\frac{m_{\mu\mu}}{m_{ss}}}$
(ii)	(16), (10), (5)	$\frac{m_{e\mu}}{m_{es}}=\frac{m_{\mu\tau}}{m_{\tau s}}=\frac{m_{\mu\mu}}{m_{\mu s}}=\frac{m_{\mu s}}{m_{ss}}=\sqrt{\frac{m_{\mu\mu}}{m_{ss}}}$
(iii)	(5), (9), (6)	$(a)\quad \frac{m_{e\mu}}{m_{\mu s}}=\frac{m_{ee}}{m_{es}},\quad (b)\quad m_{ee}m_{ss}=m_{es}^2$
(iv)	(17), (9), (6)	$(a)\quad \frac{m_{e\mu}}{m_{es}}=\frac{m_{\mu\tau}}{m_{\tau s}},\quad (b)\quad m_{ee}m_{ss}=m_{es}^2$
(v)	(18), (10), (1)	$m_{ee}(m_{\mu\mu}m_{\tau s}-m_{\mu s}m_{\mu\tau})=m_{e\mu}(m_{e\mu}m_{\tau s}-m_{es}m_{\mu\tau})$
$D_1(i)$	(19), (10), (1)	$\frac{m_{ee}}{m_{e\tau}}-\frac{m_{e\tau}}{m_{\tau\tau}}=\left(\frac{m_{ee}}{m_{\tau\tau}}-\frac{m_{e\tau}^2}{m_{\tau\tau}^2}\right)\frac{l}{c}$
(ii)	(20), (9), (6)	$(a)\quad \frac{m_{e\mu}}{m_{\mu s}}=\frac{m_{e\tau}}{m_{\tau s}},\quad (b)\quad m_{\tau\tau}m_{ss}=m_{\tau s}^2$
(iii)	(2), (10), (5)	$\frac{m_{e\mu}}{m_{\mu s}}=\frac{m_{e\tau}}{m_{\tau s}}=\sqrt{\frac{m_{ee}}{m_{ss}}}$
(iv)	(21), (9), (6)	$\frac{m_{ee}}{m_{es}}=\frac{m_{es}}{m_{ss}}=\frac{m_{e\tau}}{m_{\tau s}}=\frac{m_{e\mu}}{m_{\mu s}}=\sqrt{\frac{m_{ee}}{m_{ss}}}$
(v)	(16), (9), (6)	$(a)\quad \frac{m_{e\tau}}{m_{\tau s}}=\frac{m_{es}}{m_{ss}},\quad (b)\quad m_{ee}m_{ss}=m_{es}^2$
$D_2(i)$	(23), (10), (1)	$\frac{m_{ee}}{m_{e\mu}}-\frac{m_{e\mu}}{m_{\mu\mu}}=\left(\frac{m_{ee}}{m_{\mu\mu}}-\frac{m_{e\mu}^2}{m_{\mu\mu}^2}\right)\frac{f}{c}$
(ii)	(22), (9), (6)	$(a)\quad \frac{m_{e\tau}}{m_{\tau s}}=\frac{m_{e\mu}}{m_{\mu s}},\quad (b)\quad m_{\mu\mu}m_{ss}=m_{\mu s}^2$
(iii)	(8), (10), (5)	$\frac{m_{e\tau}}{m_{\tau s}}=\frac{m_{e\mu}}{m_{\mu s}}=\sqrt{\frac{m_{ee}}{m_{ss}}}$
(iv)	(24), (9), (6)	$\frac{m_{ee}}{m_{es}}=\frac{m_{es}}{m_{ss}}=\frac{m_{e\tau}}{m_{\tau s}}=\frac{m_{e\mu}}{m_{\mu s}}=\sqrt{\frac{m_{ee}}{m_{ss}}}$
(v)	(12), (9), (6)	$(a)\quad \frac{m_{e\mu}}{m_{\mu s}}=\frac{m_{es}}{m_{ss}},\quad (b)\quad m_{ee}m_{ss}=m_{es}^2$
$F_1(i)$	(24), (10), (2)	$m_{ee}m_{ss}=m_{es}^2$
(ii)	(21), (10), (2)	$m_{ee}m_{ss}=m_{es}^2$

(*continued on next page*)

The remaining 39 basic combinations of M_D, M_R and M_S along with their correlations are presented in Table 8. In our analysis we have found that some combinations are having multiple correlations.

Table 8 (*continued*)

Texture	M_D, M_R, M_S	Correlations
(iii)	(17), (7), (3)	$\frac{m_{\mu\tau}}{m_{\tau\tau}} = \frac{m_{\mu s}}{m_{\tau s}}$
(iv)	(13), (7), (3)	$\frac{m_{\mu\mu}}{m_{\mu\tau}} = \frac{m_{\mu s}}{m_{\tau s}}$
$F_2(i)$	(15), (10), (2)	$m_{\mu\mu} m_{ss} = m^2_{\mu s}$
(ii)	(10), (10), (2)	$m_{\mu\mu} m_{ss} = m^2_{\mu s}$
(iii)	(7), (7), (3)	$\frac{m_{ee}}{m_{es}} = \frac{m_{e\tau}}{m_{\tau s}}$
(iv)	(22), (7), (3)	$\frac{m_{e\tau}}{m_{es}} = \frac{m_{\tau\tau}}{m_{\tau s}}$
$F_3(i)$	(11), (10), (2)	$m_{\tau\tau} m_{ss} = m^2_{\tau s}$
(ii)	(3), (10), (2)	$m_{\tau\tau} m_{ss} = m^2_{\tau s}$
(iii)	(25), (7), (2)	$\frac{m_{ee}}{m_{es}} = \frac{m_{e\mu}}{m_{\mu s}}$
(iv)	(26), (7), (2)	$\frac{m_{e\mu}}{m_{es}} = \frac{m_{\mu\mu}}{m_{\mu s}}$

5. Viability of the textures

In our analysis we calculate the mass matrix elements m_{ij}, $i, j = (e, \mu, \tau$ and $s)$ using the current neutrino data (Table 1) in the expressions given in the Appendix. The range of Dirac and the Majorana CP phases is considered to be $(0-2\pi)$. The viability of a texture shall be examined under the following two conditions:

(i) The left hand side (lhs) and the right hand side (rhs) of the correlation(s) of a given texture are plotted against $\sin\theta_{34}$ in the range $(0-0.4)$. If there happens a reasonable overlapping of the plots of lhs and rhs, then the texture is considered as an allowed texture within the overlapping range of $\sin\theta_{34}$. We also study the viability of the textures when the CP phases are constrained to some random ranges of values within $(0-2\pi)$. In analysis, we categorise them as (a) CP phase dependent textures and (b) CP phase independent textures. It is to be noted that in case, a texture is having more than one correlation and at least one of them is CP phase dependent, then the texture belongs to CP phase dependent category.

(ii) The effective electron neutrino mass $|m_{\beta\beta}|$ which indicates the rate of neutrinoless double beta decay. We calculate $|m_{\beta\beta}|$ for each texture using the data in Table 1 in the following Eq. (27):

$$|m_{\beta\beta}| = |m_1 c_{12}^2 c_{13}^2 c_{14}^2 + m_2 c_{13}^2 c_{14}^2 s_{12}^2 e^{-i\alpha} + m_3 c_{14}^2 s_{13}^2 e^{-i\beta} + m_4 s_{14}^2 e^{-i\gamma}|. \quad (27)$$

For NH we put $m_1 = 0$ and for IH $m_3 = 0$. Again three Majorana CP violating phases α, β, γ are not constrained by experimental limits i.e., they may take values between 0 to 2π. There are a number of experiments [73–76] which are looking for more accurate limit on $|m_{\beta\beta}|$. The most constraint upper bound has been set to $|m_{\beta\beta}| < 0.06 - 0.165$ eV at 90% C.L. by the KamLAND ZEN Collaboration [76].

Now naturally a texture is considered to be viable if both the above conditions are satisfied simultaneously. The procedure of our analysis is the following: in the first place, we examine the textures under the condition (i) i.e., the consistency of the correlation(s) of a texture and categorize it into CP phase dependent or independent. If consistency is not found for a texture, then such texture is ruled out for not being viable. In the second place, we calculate $|m_{\beta\beta}|$ for the viable textures only under the condition (i). Again a viable texture under condition (i) may be ruled out if $|m_{\beta\beta}|$ for the texture is not within the experimental constraints.

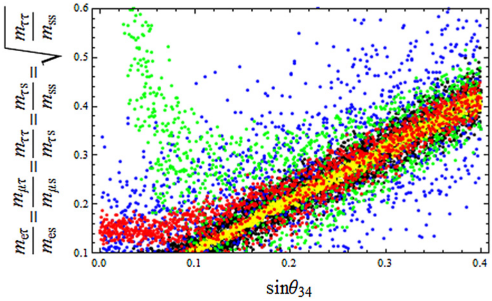

Fig. 1. Scatter plot for Eq. (20) against $\sin\theta_{34}$ for unconstrained CP phases (Texture $B_3(i)$, NH). ■ $\frac{m_{e\tau}}{m_{es}}$, ■ $\frac{m_{\mu\tau}}{m_{\mu s}}$, ■ $\frac{m_{\tau\tau}}{m_{\tau s}}$, ■ $\frac{m_{\tau s}}{m_{ss}}$, ■ $\sqrt{\frac{m_{\tau\tau}}{m_{ss}}}$. (For interpretation of the colours in the figures, the reader is referred to the web version of this article.)

In addition, we also consider to determine the Jarlskog invariant J_{CP} of a texture. For (3+1) scheme, Jarlskog invariant ($J^{4\nu}_{CP} = Im[U_{e1}U_{\mu 2}U^*_{e2}U^*_{\mu 1}]$) according to the parametrization in Eq. (6) takes the form

$$J^{4\nu}_{CP} = J^{3\nu}_{CP}c^2_{14}c^2_{24} + s_{24}s_{14}c_{24}c_{23}c^2_{14}c^3_{13}c_{12}s_{12}\sin(\delta_{14} - \delta_{24}), \tag{28}$$

where

$$J^{3\nu}_{CP} = s_{12}s_{23}s_{13}c_{12}c_{23}c^2_{13}\sin\delta_{13}. \tag{29}$$

The ranges of Dirac CP phases ($\delta_{13}, \delta_{14}, \delta_{24}$) for calculating $J^{4\nu}_{CP}$ are considered the same for which a texture becomes viable. The textures which are not consistent with the viability conditions (i) and (ii), will not be considered for calculating $J^{4\nu}_{CP}$.

5.1. CP phase dependent textures

There are two categories of CP phase dependent textures because of their phenomenology illustrated below.

Category-I: This class of textures shows overlapping of scatter plots only for partial range of $\sin\theta_{34}$ when CP phases are not constrained to any segmented range. In a systematic analysis we have found that there exist some ranges of CP phases for which overlapping of scatter plots of such textures always disappears within the range of $\sin\theta_{34} = (0 - 0.4)$. For example, one such case is presented here:

We pick up the case of the texture $B_3(i)$ in Table 8. Firstly we calculate the matrix elements m_{ij} with $i, j = (e, \mu, \tau$ and $s)$ given in the Appendix using 3σ range of the parameters of neutrino data in Table 1 and taking unconstrained CP phases in the range $(0 - 2\pi)$. We present the NH case for the texture $B_3(i)$ for which $m_1 = 0$ is set for calculation of the matrix elements. Each of 5 expressions in the correlations for $B_3(i)$ in Eq. (20) separated by equality sign is plotted against $\sin\theta_{34}$ with its range $(0 - 0.4)$. Fig. 1 shows these correlation plots.

It is evident from Fig. 1 that the correlations in Eq. (20) are consistent only for $\sin\theta_{34} > 0.1$ for unconstrained CP phases. For values of $\sin\theta_{34} < 0.1$ the overlapping of the plots for $\frac{m_{\tau\tau}}{m_{\tau s}}$ and $\sqrt{\frac{m_{\tau\tau}}{m_{ss}}}$ disappears and the texture is not allowed below that value of $\sin\theta_{34}$. This predicts a lower bound on $\sin\theta_{34}$ to be 0.1 for this texture.

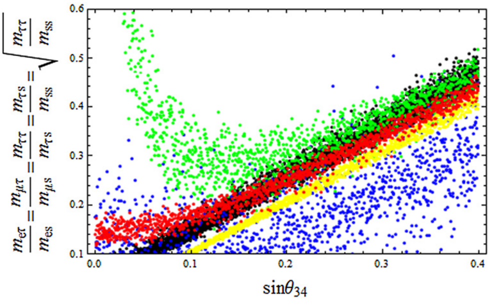

Fig. 2. Scatter plot for Eq. (20) against $\sin\theta_{34}$ for constrained ranges of CP phases: $\delta_{13} = \delta_{14} = (45^0 - 90^0)$, $\delta_{24} = (180^0 - 225^0)$, $\alpha = (135^0 - 180^0)$, $\beta = \gamma = (0 - 45^0)$ (Texture $B_3(i)$, NH). ■ $\frac{m_{e\tau}}{m_{es}}$, ■ $\frac{m_{\mu\tau}}{m_{\mu s}}$, ■ $\frac{m_{\tau\tau}}{m_{\tau s}}$, ■ $\frac{m_{\tau s}}{m_{ss}}$, ■ $\sqrt{\frac{m_{\tau\tau}}{m_{ss}}}$.

If CP phases are constrained to the ranges: $\delta_{13} = \delta_{14} = (45^0 - 90^0)$, $\delta_{24} = (180^0 - 225^0)$, $\alpha = (135^0 - 180^0)$, $\beta = \gamma = (0 - 45^0)$, the overlapping of plots completely vanishes and the texture becomes non-viable for any range of $\sin\theta_{34}$ (Fig. 2). This indicates that there is an interplay of CP phases in case of the viability of a texture. Again the textures $A_1(iii)$, (v); $B_3(i)$, (ii) (Table 8) also give the same correlations as in Eq. (20) and therefore, they show similar phenomenology with the texture $B_3(i)$. We do not consider the calculation of $m_{\beta\beta}$ for this category of textures. Inverted hierarchical case of texture $B_3(i)$ also shows similar phenomenology. The textures of Category I are listed in Table 9.

Category-II: The textures belonging to this category have the special features that their scatter plots always have reasonable overlapping in part of the range of $\sin\theta_{34}$ when CP phases are randomly constrained to some range within $0 - 2\pi$.

We present the case of $D_1(iv)$ (NH) of this category. Following the similar procedure of Category-I, we have plotted the Fig. 3. Plot (a) and Plot (b) are the correlation plots of Eq. (23) for unconstrained and constrained CP phases respectively. The figure shows that the texture is allowed for all ranges of $\sin\theta_{34} = (0.0 - 0.4)$ for unconstrained CP phases. However, on constraining the phases to their respective ranges: $\delta_{13} = (45^0 - 90^0)$, $\delta_{14} = (180^0 - 225^0)$, $\delta_{24} = (270^0 - 315^0)$, $\alpha = (270^0 - 315^0)$, $\beta = (90^0 - 135^0)$, $\gamma = (330^0 - 360^0)$, the texture is allowed for the range $(0.06 - 0.40)$ of $\sin\theta_{34}$. On surveying the correlation with different ranges of CP phases, we find that the texture is always allowed at least for some values of $\sin\theta_{34}$, unlike the Category-I, and this is true even when CP phases are made to vanish. This clearly argues for different phenomenology of Category-II from Category-I.

Table 10 shows the allowed ranges of $\sin\theta_{34}$ for the textures belonging to this Category-II with and without constraining CP phases. Their respective constrained ranges of CP phases are presented in Table 11. There is a lower limit of $\sin\theta_{34}$ for many textures observed in case of unconstrained CP phases.

Analysis under J_{CP} and $|m_{\beta\beta}|$

Now we check the compatibility of the textures which are allowed in scatter plots in context of the values of $|m_{\beta\beta}|$ under the same conditions of CP phases as imposed in case of the scatter plots. We also calculate the value of Jarlskog invariant J_{CP} for each case considering the constrained range of Dirac CP phases.

Table 9
Category-I: textures not allowed for the ranges of CP phases.

Texture	Constrained CP phases
$A_1(iii), (v)$ (NH); $B_3(i), (ii)$ (NH)	$\delta_{13} = \delta_{14} = (45^0 - 90^0)$, $\delta_{24} = (180^0 - 225^0)$, $\alpha = (135^0 - 180^0)$, $\beta = \gamma = (0 - 45^0)$
$A_1(iv)(a)$ (NH); $B_3(iv)(a)$ (NH)	$\delta_{13} = (180^0 - 225^0)$, $\delta_{14} = \delta_{24} = (0 - 30^0)$, $\alpha = (0 - 90^0)$, $\beta = (315^0 - 360^0)$, $\gamma = (270^0 - 315^0)$
$B_3(i), (ii)$ (IH)	$\delta_{13} = (45^0 - 90^0)$, $\delta_{14} = (90^0 - 135^0)$, $\delta_{24} = (0 - 45^0)$ $\alpha = (270^0 - 315^0)$, $\beta = \gamma = (0 - 30^0)$
$B_3(iii)(a)$ (IH)	$\delta_{13} = (0 - 90^0)$, $\delta_{14} = (90^0 - 130^0)$, $\delta_{24} = (0 - 180^0)$ $\alpha = (0 - 30^0)$, $\beta = (0 - 180^0)$, $\gamma = (0 - 90^0)$
$B_3(iv)(a)$ (NH, IH)	$\delta_{13} = (180^0 - 225^0)$, $\delta_{14} = (225^0 - 270^0)$, $\delta_{24} = (180^0 - 210^0)$ $\alpha = \gamma = (180^0 - 225^0)$, $\beta = (225^0 - 270^0)$
$B_3(v)$ (IH)	$\delta_{13} = (0 - 90^0)$, $\delta_{14} = \delta_{24} = (325^0 - 360^0)$ $\alpha = (0 - 45^0)$, $\beta = (45^0 - 90^0)$, $\gamma = (0 - 90^0)$
$B_4(iv)(a)$ (IH)	$\delta_{13} = (0 - 90^0)$, $\delta_{14} = (90^0 - 180^0)$, $\delta_{24} = (45^0 - 90^0)$ $\alpha = (0 - 45^0)$, $\beta = \gamma = (0 - 30^0)$
$D_1(ii)(a)$ (IH); $D_2(ii)(a)$ (IH)	$\delta_{13} = (0 - 45^0)$, $\delta_{14} = \delta_{24} = (0 - 30^0)$, $\alpha = (270^0 - 315^0)$, $\beta = (130^0 - 180^0)$, $\gamma = (225^0 - 270^0)$
$D_1(iii)$ (IH)	$\delta_{13} = (45^0 - 90^0)$, $\delta_{14} = (0 - 30^0)$, $\delta_{24} = (315^0 - 360^0)$ $\alpha = (0 - 45^0)$, $\beta = (0 - 30^0)$, $\gamma = (315^0 - 360^0)$
$D_1(iv)$ (IH)	$\delta_{13} = \delta_{24} =$ unconstrained, $\delta_{14} = (0 - 270^0)$ $\alpha = (0 - 90^0)$, $\beta = (0 - 90^0)$, $\gamma = (0 - 30^0)$
$D_2(v)(a)$ (IH)	$\delta_{13} = (45^0 - 90^0)$, $\delta_{14} = \delta_{24} = (0 - 45^0)$ $\alpha = \gamma = (180^0 - 225^0)$, $\beta = (0 - 45^0)$
$F_3(iii)$ (IH)	$\delta_{13} = (45^0 - 90^0)$, $\delta_{14} = (315^0 - 360^0)$, $\delta_{24} = \alpha = (0 - 30^0)$ $\alpha = (0 - 30^0)$, $\beta = (90^0 - 135^0)$, $\gamma = (270^0 - 315^0)$

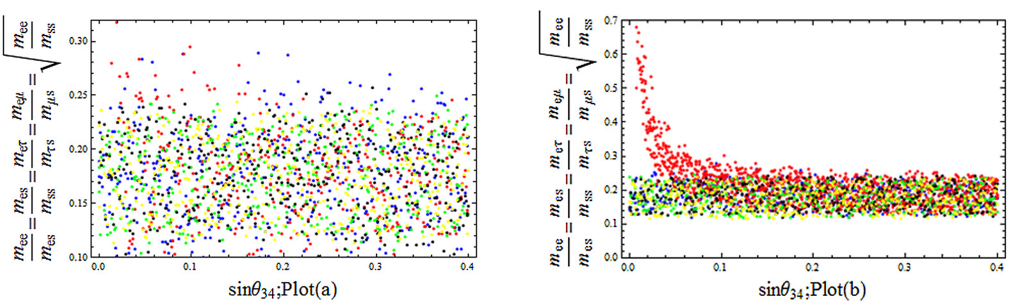

Fig. 3. Scatter plot for Eq. (23) against $\sin\theta_{34}$ for unconstrained (Plot (a)) and constrained (Plot (b)) ranges of CP phases: $\delta_{13} = (45^0 - 90^0)$, $\delta_{14} = (180^0 - 225^0)$, $\delta_{24} = (270^0 - 315^0)$, $\alpha = (270^0 - 315^0)$, $\beta = (90^0 - 135^0)$, $\gamma = (330^0 - 360^0)$ (Texture $D_1(iv)$, NH). ■ $\frac{m_{ee}}{m_{es}}$, ■ $\frac{m_{es}}{m_{ss}}$, ■ $\frac{m_{e\tau}}{m_{\tau s}}$, ■ $\frac{m_{e\mu}}{m_{\mu s}}$, ■ $\sqrt{\frac{m_{ee}}{m_{ss}}}$.

Table 10
Table shows the allowed range of $\sin\theta_{34}$ for unconstrained and constrained CP phases for textures under Category (II). Here '*All*' represents that the texture allows all values of $\sin\theta_{34} = (0 - 0.4)$.

Texture	Range of $\sin\theta_{34}$ for	
	unconstrained CP	constrained CP
$A_1(i)$ (NH)	$(0.04 - 0.4)$	$(0.08 - 0.4)$
$A_1(ii)(a)$ (NH)	> 0.02	$(0.02 - 0.1)$
$A_2(ii)(a)$ (NH)	> 0.08	> 0.1
$A_2(ii)(b)$ (NH)	> 0.08	> 0.12
$A_2(iii), (v)$ (NH)	> 0.04	> 0.08
$A_2(iv)(a)$ (NH)	> 0.04	> 0.14
$B_3(iii)(a)$ (NH)	*All*	> 0.2
$B_3(v)$ (NH)	*All*	> 0.06
$B_4(iv)(a)$ (NH)	> 0.02	< 0.06
$B_4(iv)(a)$ (IH)	> 0.02	< 0.18
$B_4(v)$ (NH)	*All*	< 0.14
$B_4(v)$ (IH)	*All*	< 0.06
$D_1(ii)(a)$ (NH)	> 0.02	> 0.1
$D_1(iii)$ (NH)	*All*	> 0.04
$D_1(iv)$ (NH)	*All*	> 0.06
$D_1(v)(a)$ (NH)	> 0.02	> 0.06
$D_1(v)(a)$ (IH)	> 0.06	> 0.24
$F_1(iii)$ (NH)	> 0.04	> 0.1
$F_1(iii)$ (IH)	> 0.04	> 0.32
$F_1(iv)$ (IH)	> 0.04	$(0.02 - 0.06)$
$F_2(iv)$ (NH)	> 0.1	> 0.14
$F_2(iv)$ (IH)	> 0.04	$(0.04 - 0.06)$

Table 11
Constrained ranges of CP phases for textures under Category-(II). The third column represents the value of $|m_{\beta\beta}|$ and J_{CP} for constrained ranges of Majorana CP phases (α, β, γ) and Dirac CP phases $(\delta_{13}, \delta_{14}, \delta_{24})$ respectively. For the textures A_1, A_2, the element $m_{ee} = 0$. This is represented as '–' for $|m_{\beta\beta}|$ in the table.

Texture	Constrained ranges of CP phases	$\lvert m_{\beta\beta}\rvert$ (eV) & J_{CP}
$A_1(i)$ (NH)	$\alpha = \gamma = (225^0 - 270^0)$, $\beta = (135^0 - 180^0)$ $\delta_{13} = (45^0 - 90^0)$, $\delta_{14} = (180^0 - 225^0)$, $\delta_{24} = (0 - 45^0)$	$\lvert m_{\beta\beta}\rvert = -$ $J_{CP} = (0 - 0.02)$
$A_1(ii)(a)$ (NH)	$\alpha = (0 - 45^0)$, $\beta = (0 - 30^0)$, $\gamma = (120^0 - 160^0)$ $\delta_{13} = (135^0 - 180^0)$, $\delta_{14} = (325^0 - 360^0)$, $\delta_{24} = (90^0 - 135^0)$	– $(0 - 0.02)$
$A_2(ii)(a)$ (NH)	$\alpha = (225^0 - 270^0)$, $\beta = (180^0 - 225^0)$, $\gamma = (315^0 - 360^0)$ $\delta_{13} = (135^0 - 180^0)$, $\delta_{14} = (225^0 - 270^0)$, $\delta_{24} = (270^0 - 315^0)$	– $(0 - 0.02)$
$A_2(ii)(b)$ (NH)	$\alpha = (225^0 - 270^0)$, $\beta = (0 - 45^0)$, $\gamma = (0 - 30^0)$ $\delta_{13} = (0 - 30^0)$, $\delta_{14} = (225^0 - 270^0)$, $\delta_{24} = (0 - 45^0)$	– $(0 - 0.02)$
$A_2(iii), (v)$ (NH)	$\alpha = (315^0 - 360^0)$, $\beta = \gamma = (0 - 30^0)$ $\delta_{13} = (45^0 - 90^0)$, $\delta_{14} = (180^0 - 225^0)$, $\delta_{24} = (180^0 - 225^0)$	– $(0.02 - 0.04)$
$A_2(iv)(a)$ (NH)	$\alpha = (135^0 - 180^0)$, $\beta = (0 - 30^0)$, $\gamma = (315^0 - 360^0)$ $\delta_{13} = (180^0 - 225^0)$, $\delta_{14} = \delta_{24} = (0 - 30^0)$	– $(0 - 0.02)$

Table 11 (*continued*)

Texture	Constrained ranges of CP phases	$\|m_{\beta\beta}\|$ (eV) & J_{CP}
$B_3(iii)(a)$ (NH)	$\alpha = (315^0 - 360^0)$, $\beta = \gamma = (330^0 - 360^0)$ $\delta_{13} = (160^0 - 200^0)$, $\delta_{14} = (330^0 - 360^0)$, $\delta_{24} = (180^0 - 225^0)$	(0.02 – 0.07) (0 – 0.02)
$B_3(v)$ (NH)	$\alpha = (180^0 - 225^0)$, $\beta = \gamma = (315^0 - 360^0)$ $\delta_{13} = \delta_{24} < 45^0$, $\delta_{14} = (90^0 - 135^0)$	(0.01 – 0.06) (0.004 – 0.04)
$B_4(iv)(a)$ (NH)	$\alpha = (180^0 - 225^0)$, $\beta = \gamma = (315^0 - 360^0)$ $\delta_{13} = (180^0 - 225^0)$, $\delta_{14} = (0 - 20^0)$, $\delta_{24} = (180^0 - 200^0)$	(0.01 – 0.06) (0 – 0.025)
$B_4(iv)(a)$ (IH)	$\alpha = \beta = (315^0 - 360^0)$, $\gamma = (270^0 - 360^0)$ $\delta_{13} = (180^0 - 225^0)$, $\delta_{14} = \delta_{24} = (0 - 30^0)$	(0.05 – 0.1) (0 – 0.03)
$B_4(v)$ (NH)	$\alpha = \gamma = (30^0 - 45^0)$, $\beta = (225^0 - 270^0)$ $\delta_{13} = (0 - 45^0)$, $\delta_{14} = (0 - 10^0)$, $\delta_{24} = (45^0 - 90^0)$	(0.02 – 0.07) (0 – 0.02)
$B_4(v)$ (IH)	$\alpha = (0 - 45^0)$, $\beta = \gamma = (0 - 30^0)$ $\delta_{13} = (90^0 - 180^0)$, $\delta_{14} = \delta_{24} = (0 - 30^0)$	(0.06 – 0.1) (0 – 0.04)
$D_1(ii)(a)$ (NH)	$\alpha = (135^0 - 180^0)$, $\beta = \gamma = (315^0 - 360^0)$ $\delta_{13} = (0 - 45^0)$, $\delta_{14} = (0 - 30^0)$, $\delta_{24} = (45^0 - 90^0)$	(0.01 – 0.06) (0 – 0.02)
$D_1(iii)$ (NH)	$\alpha = (315^0 - 360^0)$, $\beta = (270^0 - 315^0)$, $\gamma = (135^0 - 180^0)$ $\delta_{13} = (135^0 - 180^0)$, $\delta_{14} = (0 - 30^0)$, $\delta_{24} = (270^0 - 300^0)$	(0.005 – 0.06) (0 – 0.04)
$D_1(iv)$ (NH)	$\alpha = (180^0 - 225^0)$, $\beta = (90^0 - 135^0)$, $\gamma = (330^0 - 360^0)$ $\delta_{13} = (45^0 - 90^0)$, $\delta_{14} = \delta_{24} = (270^0 - 315^0)$	(0.01 – 0.06) (0 – 0.05)
$D_1(v)(a)$ (NH)	$\alpha = (135^0 - 180^0)$, $\beta = (0 - 30^0)$, $\gamma = (225^0 - 315^0)$ $\delta_{13} = (45^0 - 90^0)$, $\delta_{14} = (315^0 - 360^0)$, $\delta_{24} = (0 - 30^0)$	(0.01 – 0.06) (0.01 – 0.04)
$D_1(v)(a)$ (IH)	$\alpha = (90^0 - 135^0)$, $\beta = (0 - 30^0)$, $\gamma = (135^0 - 180^0)$ $\delta_{13} = (45^0 - 90^0)$, $\delta_{14} = (180^0 - 225^0)$, $\delta_{24} = (225^0 - 270^0)$	(0.01 – 0.05) (0.01 – 0.04)
$F_1(iii)$ (NH)	$\alpha = (270^0 - 315^0)$, $\beta = (180^0 - 225^0)$, $\gamma = (315^0 - 360^0)$ $\delta_{13} = (135^0 - 180^0)$, $\delta_{14} = \delta_{24} = (225^0 - 270^0)$	(0.02 – 0.07) (0 – 0.02)
$F_1(iii)$ (IH)	$\gamma = \beta = \alpha = (0 - 30^0)$ $\delta_{13} = \delta_{24} = (0 - 45^0)$, $\delta_{14} = (180^0 - 225^0)$	(0.03 – 0.1) (0 – 0.03)
$F_1(iv)$ (IH)	$\alpha = \beta = (0 - 45^0)$, $\gamma = (0 - 30^0)$ $\delta_{13} = (0 - 90^0)$, $\delta_{14} = (0 - 30^0)$, $\delta_{24} = (0 - 45^0)$	(0.06 – 0.11) (0 – 0.04)
$F_2(iv)$ (NH)	$\gamma = \beta = \alpha = (315^0 - 360^0)$ $\delta_{13} = (0 - 45^0)$, $\delta_{14} = \delta_{24} = (0 - 30^0)$	(0.02 – 0.07) (0 – 0.03)
$F_2(iv)$ (IH)	$\alpha = (180^0 - 225^0)$, $\beta = (0 - 30^0)$, $\gamma = (0 - 45^0)$ $\delta_{13} = (45^0 - 90^0)$, $\delta_{14} = (0 - 30^0)$, $\delta_{24} = (180^0 - 225^0)$	(0.03 – 0.08) (0.02 – 0.04)

Here we consider $D_1(iv)$ (NH) as a representative case for illustration. We show the variation of $|m_{\beta\beta}|$ and J_{CP} (Fig. 5) for the constrained ranges of Majorana CP phases $\alpha = (270^0 - 315^0)$, $\beta = (90^0 - 135^0)$, $\gamma = (330^0 - 360^0)$ and Dirac CP phases $\delta_{13} = (45^0 - 90^0)$, $\delta_{14} = (180^0 - 225^0)$, $\delta_{24} = (270^0 - 315^0)$ respectively. For unconstrained CP phases, we obtain $|m_{\beta\beta}| \approx (0.01 - 0.06)$ eV for NH and $\approx (10^{-3} - 0.1)$ eV for IH (Fig. 4). In Fig. 5 (left plot), we study the dependence of $|m_{\beta\beta}|$ on the lightest neutrino mass for constrained range of

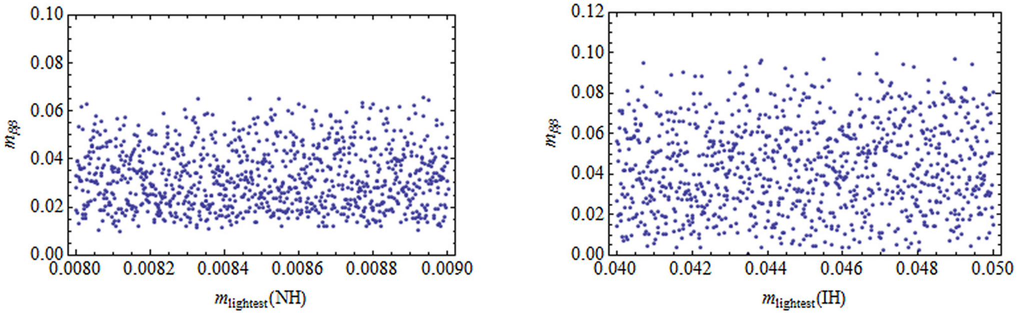

Fig. 4. Scatter plot for $|m_{\beta\beta}|$ for Normal Hierarchy (left plot) and Inverted Hierarchy (right plot) for unconstrained CP phases.

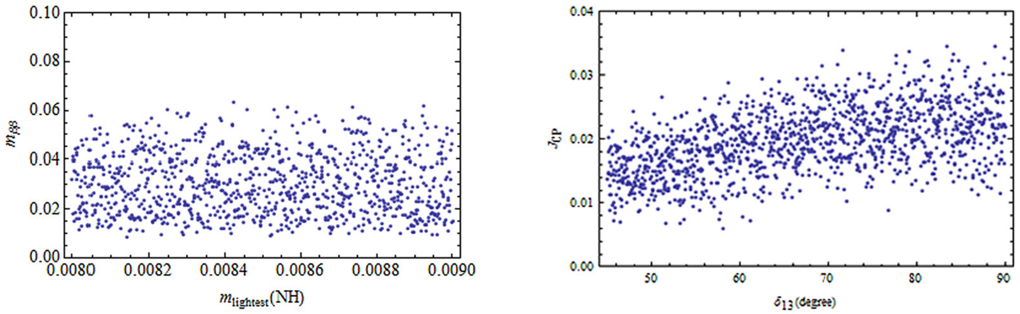

Fig. 5. Scatter plot for $|m_{\beta\beta}|$ (left plot) and J_{CP} (right plot) for constrained ranges of CP phases: $\alpha = (270^0 - 315^0)$, $\beta = (90^0 - 135^0)$, $\gamma = (330^0 - 360^0)$ and $\delta_{13} = (45^0 - 90^0)$, $\delta_{14} = (180^0 - 225^0)$, $\delta_{24} = (270^0 - 315^0)$ (Texture $D_1(iv)$, NH).

Majorana CP phases ($\alpha = (270^0 - 315^0)$, $\beta = (90^0 - 135^0)$, $\gamma = (330^0 - 360^0)$). Accordingly we present the parameter space of $|m_{\beta\beta}|$ with respect to the lightest neutrino mass ($m_{lightest}$) in left plot of Fig. 5 for normal hierarchy (NH) pattern. As demanded by MES mechanism, for NH $m_1 = 0$. In our analysis, we have plotted $|m_{\beta\beta}|$ against m_2 for NH pattern. Similarly for cases with inverted hierarchy $|m_{\beta\beta}|$ is obtained against m_1 (as $m_2 > m_1$ and $m_3 = 0$ according to MES mechanism). From Fig. 5 it is evident that for the constrained range of α, β, γ, the texture predicts $|m_{\beta\beta}| \approx (0.01 - 0.06)$ eV which lies below the upper bound of $|m_{\beta\beta}| < 0.061 - 0.165$ [76]. Hence, we consider this texture with the above constrained CP phases to be an allowed texture. Again, we find that for unconstrained Dirac CP phases, the Jarlskog invariant J_{CP} which provides a measure of the Dirac-type CP violation is $J_{CP} \approx (0 - 0.05)$ for both NH and IH and the maximal value of $J_{CP} \approx 0.05$ is for $\delta_{13} = 90^0$ and 270^0. From Fig. 5 (right plot) it is seen that for constrained range of Dirac CP phases $\delta_{13} = (45^0 - 90^0)$, $\delta_{14} = (180^0 - 225^0)$, $\delta_{24} = (270^0 - 315^0)$, $J_{CP} = (0.01 - 0.03)$. The range of $|m_{\beta\beta}|$ and J_{CP} for constrained ranges of CP phases for textures under Category-II are presented in Table 11.

5.2. *CP phase independent textures*

The textures $A_2(i)$ and $B_4(iii)$ among all the textures remain viable for the whole range of $\sin\theta_{34} = (0.0 - 0.4)$ whether CP phases are unconstrained or constrained to different ranges, or

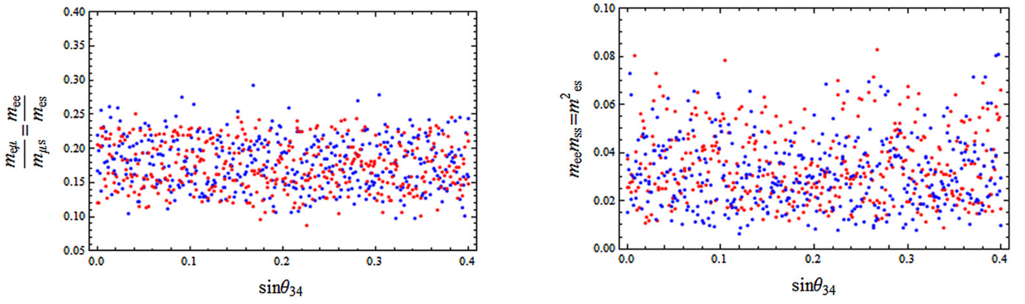

Fig. 6. Scatter plots of texture $B_4(iii)$ for Eq. (25) (left plot) and Eq. (26) (right plot) against $\sin\theta_{34}$ for unconstrained CP phases. ■ $\frac{m_{e\mu}}{m_{\mu s}}$, ■ $\frac{m_{ee}}{m_{es}}$ (left plot) and ■ $m_{ee}m_{ss}$, ■ m_{es}^2 (right plot).

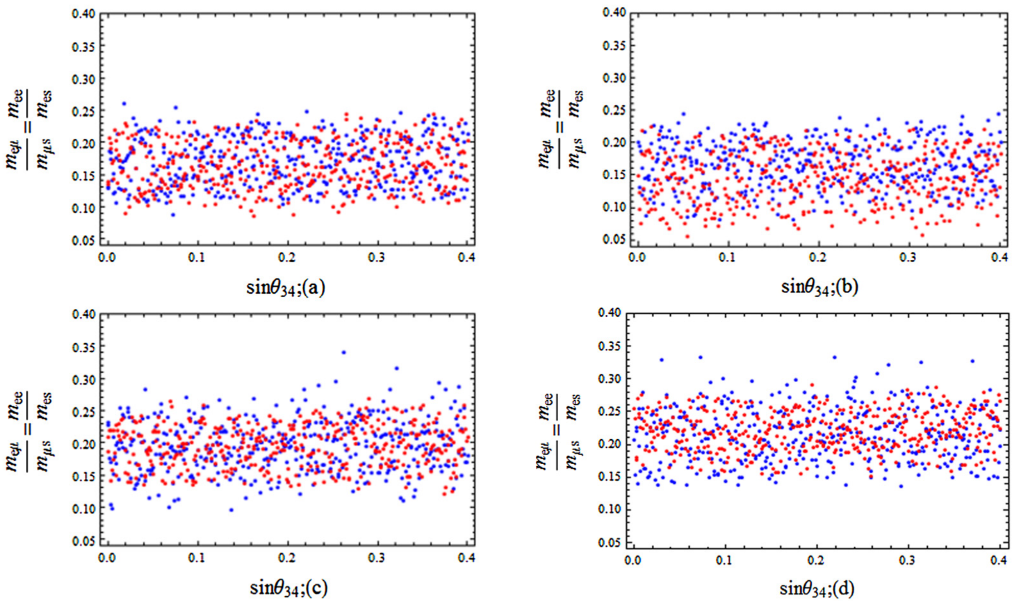

Fig. 7. Scatter plot of texture $B_4(iii)$ for Eq. (25) against $\sin\theta_{34}$ for constrained ranges of CP phases: Plot (a) is for: $\delta_{13} = \beta = (45^0 - 90^0)$, $\gamma < 30^0$, $\delta_{14} = (90^0 - 130^0)$, $\delta_{24} = (180^0 - 270^0)$, $\alpha = (270^0 - 360^0)$. Plot (b) for: $\delta_{13} = \gamma = (135^0 - 180^0)$, $\beta = (45^0 - 90^0)$, $\delta_{14} = (180^0 - 225^0)$, $\delta_{24} = (0 - 45^0)$, $\alpha = (180^0 - 270^0)$. Plot (c) for: $\delta_{13} = \gamma = (135^0 - 180^0)$, $\beta = (225^0 - 270^0)$, $\delta_{14} = (180^0 - 225^0)$, $\delta_{24} = (0 - 45^0)$, $\alpha = (0 - 30^0)$. Plot (d) for: $\delta_{13} = (0 - 30^0)$, $\gamma = (225^0 - 270^0)$, $\beta = (135^0 - 180^0)$, $\delta_{14} = (225^0 - 270^0)$, $\delta_{24} = (45^0 - 90^0)$, $\alpha = (90^0 - 135^0)$. ■ $\frac{m_{e\mu}}{m_{\mu s}}$, ■ $\frac{m_{ee}}{m_{es}}$.

even CP phases enforced to be zero. For illustration, we take the texture $B_4(iii)$. The texture has two colateral correlations Eq. (25) and Eq. (26). The Fig. 6 represents the scatter plot for Eq. (25) (left plot) and for Eq. (26) (right plot) for unconstrained CP phases. Again the Fig. 7 and 8 show the scatter plots for different chosen ranges of CP phases for Eq. (25) and (26) respectively. It is observed that the overlapping of the plots for the left-hand side and right-hand side retains even for the choice of different ranges of CP phases, thereby showing no dependence of CP phase change. Thus it is a CP phase independent texture. Similar phenomenology of CP phase independence is shown by the texture $A_2(i)$.

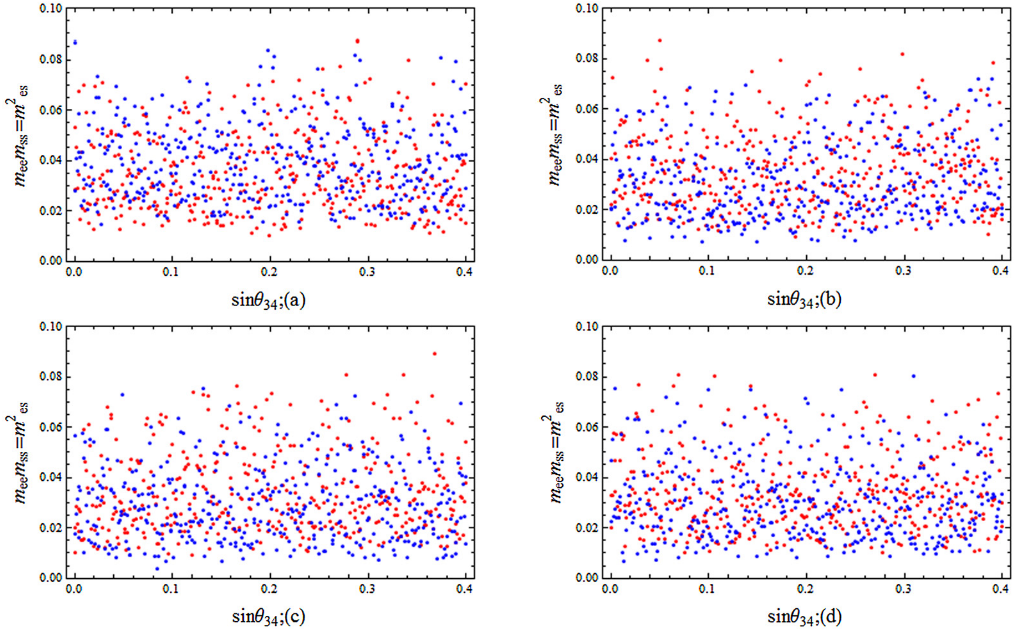

Fig. 8. Scatter plot of texture $B_4(iii)$ for Eq. (26) against $\sin\theta_{34}$ for constrained ranges of CP phases: Plot (a) is for: $\delta_{13} = \beta = (45^0 - 90^0)$, $\gamma < 30^0$, $\delta_{14} = (90^0 - 130^0)$, $\delta_{24} = (180^0 - 270^0)$, $\alpha = (270^0 - 360^0)$. Plot (b) for: $\delta_{13} = \gamma = (135^0 - 180^0)$, $\beta = (45^0 - 90^0)$, $\delta_{14} = (180^0 - 225^0)$, $\delta_{24} = (0 - 45^0)$, $\alpha = (180^0 - 270^0)$. Plot (c) for: $\delta_{13} = \gamma = (135^0 - 180^0)$, $\beta = (225^0 - 270^0)$, $\delta_{14} = (180^0 - 225^0)$, $\delta_{24} = (0 - 45^0)$, $\alpha = (0 - 30^0)$. Plot (d) for: $\delta_{13} = (0 - 30^0)$, $\gamma = (225^0 - 270^0)$, $\beta = (135^0 - 180^0)$, $\delta_{14} = (225^0 - 270^0)$, $\delta_{24} = (45^0 - 90^0)$, $\alpha = (90^0 - 135^0)$. ■ $m_{ee}m_{ss}$, ■ m^2_{es}.

Table 12
Table shows the value of $|m_{\beta\beta}|$ and J_{CP} obtained for different constrained ranges of CP phases considered in Fig. 7 and 8.

Constrained ranges of CP phases	$\|m_{\beta\beta}\|$ (eV) & J_{CP}
$\alpha = (270^0 - 360^0)$, $\beta = (45^0 - 90^0)$, $\gamma < 30^0$ $\delta_{13} = (45^0 - 90^0)$, $\delta_{14} = (90^0 - 130^0)$, $\delta_{24} = (180^0 - 270^0)$	$\|m_{\beta\beta}\| = (0.015 - 0.07)$ eV $J_{CP} = (0.01 - 0.03)$
$\alpha = (180^0 - 270^0)$, $\beta = (45^0 - 90^0)$, $\gamma = (135^0 - 180^0)$ $\delta_{13} = (135^0 - 180^0)$, $\delta_{14} = (180^0 - 225^0)$, $\delta_{24} = (0 - 45^0)$	$(0.01 - 0.06)$ $(0 - 0.03)$
$\alpha = (0 - 30^0)$, $\beta = (225^0 - 270^0)$, $\gamma = (135^0 - 180^0)$ $\delta_{13} = (135^0 - 180^0)$, $\delta_{14} = (180^0 - 225^0)$, $\delta_{24} = (0 - 45^0)$	$(0.01 - 0.06)$ $(0 - 0.03)$
$\alpha = (90 - 135^0)$, $\beta = (135^0 - 180^0)$, $\gamma = (225^0 - 270^0)$ $\delta_{13} = (0 - 30^0)$, $\delta_{14} = (225^0 - 270^0)$, $\delta_{24} = (45^0 - 90^0)$	$(0.01 - 0.06)$ $(0 - 0.02)$

We also check the range of $|m_{\beta\beta}|$ for different constrained ranges of the Majorana CP phases and found that for all the cases, the range of $|m_{\beta\beta}|$ lies within the experimental upper bound $|m_{\beta\beta}| < 0.06 - 0.165$ [76]. Similarly we also calculate the range of J_{CP} for each case of constrained Dirac CP phases. In Table 12 we have presented the values of $|m_{\beta\beta}|$ and J_{CP} for the different ranges of constrained CP phases considered in the plots of Fig. 7 and 8.

6. Symmetry realization

For every set of the fermion mass matrices with texture zeros in arbitrary entries, there corresponds to a scalar sector such that the texture zeros can always be realized by the Abelian flavor symmetries [47,48]. In the paper [48] the author discussed two methods for symmetry realization of texture zeros in the lepton sector in the framework of the seesaw mechanism. Now we adopt the method-2 of the paper for symmetry realization of the textures in our present context of MES mechanism. In doing so, the charged lepton mass matrix M_l shall be considered to be diagonal. In our systematic study, we find that Z_8 is successful for generating all the viable textures. Z_8 consists of the group elements

$$(1, \omega, \omega^2, \omega^3, \omega^4, \omega^5, \omega^6, \omega^7)$$

where $\omega = e^{\frac{i2\pi}{8}}$ is the generator of the group. We show the symmetry realization for texture $B_3(i)$ as a representative case. The leptonic fields are considered to transform under Z_8 as

$$\begin{aligned} \bar{D}_{e_L} &\to \omega^7 \bar{D}_{e_L}, & e_R &\to \omega^3 e_R, & \nu_{e_R} &\to \omega \nu_{e_R}, \\ \bar{D}_{\mu_L} &\to \omega \bar{D}_{\mu_L}, & \mu_R &\to \omega^2 \mu_R, & \nu_{\mu_R} &\to \omega^7 \nu_{\mu_R}, \\ \bar{D}_{\tau_L} &\to \omega^2 \bar{D}_{\tau_L}, & \tau_R &\to \omega^6 \tau_R, & \nu_{\tau_R} &\to \omega^3 \nu_{\tau_R}. \end{aligned} \tag{30}$$

Here, $\bar{D}_{j_L}$, l_R and ν_{k_R} represent the $SU(2)_L$ doublets, the RH $SU(2)_L$ singlets and the RH neutrino singlets respectively. The bilinears $\bar{D}_{j_L} l_R$, $\bar{D}_{j_L} \nu_{k_R}$, $\nu_{k_R}^T C^{-1} \nu_{j_R}$ relevant for M_l, M_D and M_R respectively transform as

$$\begin{aligned} &\bar{D}_{k_L} l_{j_R} = \begin{pmatrix} \omega^2 & \omega & \omega^5 \\ \omega^4 & \omega^3 & \omega^7 \\ \omega^5 & \omega^4 & 1 \end{pmatrix}, \quad \bar{D}_{k_L} \nu_{j_R} = \begin{pmatrix} 1 & \omega^6 & \omega^2 \\ \omega^2 & 1 & \omega^4 \\ \omega^3 & \omega & \omega^5 \end{pmatrix}, \\ &\nu_{k_R}^T C^{-1} \nu_{j_R} = \begin{pmatrix} \omega^2 & 1 & \omega^4 \\ 1 & \omega^6 & \omega^2 \\ \omega^4 & \omega^2 & \omega^6 \end{pmatrix}. \end{aligned} \tag{31}$$

We consider three $SU(2)_L$ doublet Higgs (Φ_1, Φ_2, Φ_3) transforming under Z_8 as

$$\Phi_1 \to \Phi_1, \qquad \Phi_2 \to \omega^6 \Phi_2, \qquad \Phi_3 \to \omega^5 \Phi_3. \tag{32}$$

The Z_8 invariant Yukawa Lagrangian becomes

$$\begin{aligned} -\mathcal{L} = {} & Y_{11}^l \bar{D}_{e_L} \Phi_2 e_R + Y_{22}^l \bar{D}_{\mu_L} \Phi_3 \mu_R + Y_{33}^l \bar{D}_{\tau_L} \Phi_1 \tau_R + Y_{11}^D \bar{D}_{e_L} \tilde{\Phi}_1 \nu_{e_R} + Y_{12}^D \bar{D}_{e_L} \tilde{\Phi}_2 \nu_{\mu_R} \\ & + Y_{22}^D \bar{D}_{\mu_L} \tilde{\Phi}_1 \nu_{\mu_R} + Y_{33}^D \bar{D}_{\tau_L} \tilde{\Phi}_3 \nu_{\tau_R} + h.c. \end{aligned} \tag{33}$$

After acquiring a non-zero vacuum expectation value $< \phi_0 > \neq 0$ by the Higgs fields, M_l and M_D take the form

$$M_l = \begin{pmatrix} m_e & 0 & 0 \\ 0 & m_\mu & 0 \\ 0 & 0 & m_\tau \end{pmatrix}, \qquad M_D = \begin{pmatrix} a & b & 0 \\ 0 & e & 0 \\ 0 & 0 & l \end{pmatrix}. \tag{34}$$

We consider a scalar singlet χ transforming under Z_8 as

$$\chi \to \omega^6 \chi, \tag{35}$$

which leads to the following form of M_R

$$M_R = \begin{pmatrix} A & B & 0 \\ B & 0 & E \\ 0 & E & 0 \end{pmatrix}. \tag{36}$$

We also consider transformation of the singlet chiral field 'S', so as to prevent bare mass term of the form $\bar{S}^c S$.

$$S \to \omega^5 S. \tag{37}$$

Scalar singlet λ_1 transforming as

$$\lambda_1 \to \lambda_1 \tag{38}$$

leads to the following form of M_S

$$M_S = \begin{pmatrix} 0 & 0 & s_3 \end{pmatrix}, \tag{39}$$

which are the zero textures of the mass matrices in Eq. (18) for texture B_3.

It has been observed that, symmetry realization of the other five S_3 symmetric textures (Table 5) of the basic combination in Eq. (18) follows an interesting pattern. For instance, considering the textures in Case (b) of Table 5 obtained by transforming the basic combination Eq. (18) by the element "B" of the S_3 group, where

$$B = \begin{pmatrix} 0 & 0 & 1 \\ 0 & 1 & 0 \\ 1 & 0 & 0 \end{pmatrix}. \tag{40}$$

There exists an interchange of the first and third column of the matrix "B". Following the similar pattern for symmetry realization of the textures of Case (b) (Table 5), and interchanging only the Z_8 transformation of the right-handed neutrino singlets ($\nu_{e_R} \Leftrightarrow \nu_{\tau_R}$) of the basic combination in Eq. (30), that is

$$\nu_{e_R} \to \omega^3 \nu_{e_R}, \quad \nu_{\tau_R} \to \omega \nu_{\tau_R}, \tag{41}$$

meanwhile keeping the transformation of all the other fields, that is, ν_{μ_R}, $\bar{D}_{j_L}$, l_R, Φ, S, χ and λ same as that of basic combination, we arrive at the following set of matrices

$$M_D = \begin{pmatrix} 0 & b & c \\ 0 & e & 0 \\ g & 0 & 0 \end{pmatrix}, \quad M_R = M_R^{(3)}, \quad M_s^{(4)} = \begin{pmatrix} s_1 & 0 & 0 \end{pmatrix}. \tag{42}$$

Similarly, symmetry realization of all the other combinations (Table 5) can be obtained by simply interchanging the transformation of the RH neutrino singlets of the basic combination, according to the interchange of the columns of the elements of the S_3 group via which the combinations are obtained. A similar study was performed in Ref. [65].

In Table 13, we present the symmetry realization of all the basic combinations of M_D, M_R and M_S. The basic combinations for each texture involves only three basic forms of the right-handed Majorana mass matrix $M_R = M_R^{(7)}, M_R^{(9)}, M_R^{(10)}$. For those textures which are realized via $M_R^{(9)}$, we keep the Z_8 transformation of the RH neutrino singlets ν_{k_R} to be the same as in Eq. (30). The transformation for the scalar singlet χ, therefore, remains the same as in Eq. (35).

For textures obtained via $M_R^{(10)}$, we consider the transformation of the RH neutrino singlets and scalar singlet χ as:

Table 13
Z_8 symmetry realization of all the basic cases.

Texture	$\bar{D}_{e_L}, \bar{D}_{\mu_L}, \bar{D}_{\tau_L}$	e_R, μ_R, τ_R	Φ's	S	$\lambda's$
$A_1(i)$	$\omega^7, \omega^3, \omega^2$	$\omega, \omega^4, \omega^7$	$1, \omega, \omega^7$	ω^2	ω, ω^7
(ii)	$\omega, \omega^2, \omega^5$	$\omega^4, \omega^6, \omega^5$	$1, \omega^3, \omega^6$	ω^5	1
(iii)	$\omega, \omega^2, \omega^5$	$\omega^7, \omega^5, 1$	$1, \omega^3, \omega$	ω^5	1
(iv)	$\omega^4, \omega^7, \omega$	$1, \omega^6, \omega^7$	$1, \omega^4, \omega^3$	ω^5	1
(v)	$\omega^7, \omega^2, \omega$	$\omega, \omega^3, 1$	$1, \omega^3, \omega^7$	ω^2	ω^7
$A_2(i)$	$\omega^7, \omega^2, \omega^3$	$\omega, \omega^7, \omega^4$	$1, \omega, \omega^7$	ω^2	ω, ω^7
(ii)	$\omega, \omega^5, \omega^2$	$\omega^4, \omega^5, \omega^6$	$1, \omega^3, \omega^6$	ω^5	1
(iii)	$\omega, \omega^5, \omega^2$	$\omega^7, 1, \omega^5$	$1, \omega^3, \omega$	ω^2	ω^7
(iv)	$\omega^4, \omega, \omega^7$	$1, \omega^7, \omega^6$	$1, \omega^4, \omega^3$	ω^5	1
(v)	$\omega^7, \omega, \omega^2$	$\omega, 1, \omega^3$	$1, \omega^3, \omega^7$	ω^5	1
$B_3(i)$	$\omega^7, \omega, \omega^2$	$\omega^3, \omega^2, \omega^6$	$1, \omega^6, \omega^5$	ω^5	1
(ii)	$\omega^7, \omega^2, \omega$	$\omega, \omega^2, \omega^4$	$1, \omega^4, \omega^3$	ω^2	ω^7
(iii)	$\omega^4, \omega, \omega^5$	$\omega^4, \omega^2, \omega^5$	$1, \omega^5, \omega^6$	ω^5	1
(iv)	$\omega^7, \omega, \omega^4$	$\omega^6, \omega^7, \omega^5$	$1, \omega^7, \omega^3$	ω^5	1
(v)	$\omega^3, \omega^7, \omega^2$	$\omega^4, \omega, \omega^7$	$1, \omega, \omega^7$	ω^2	ω, ω^7
$B_4(i)$	$\omega^7, \omega^2, \omega$	$\omega^3, \omega^6, \omega^2$	$1, \omega^6, \omega^5$	ω^5	1
(ii)	$\omega^7, \omega, \omega^2$	$\omega, \omega^4, \omega^2$	$1, \omega^4, \omega^3$	ω^2	ω^7
(iii)	$\omega^4, \omega^5, \omega$	$\omega^4, \omega^5, \omega^2$	$1, \omega^5, \omega^6$	ω^5	1
(iv)	$\omega^7, \omega^4, \omega$	$\omega^6, \omega^5, \omega^7$	$1, \omega^2, \omega^3$	ω^5	1
(v)	$\omega^3, \omega^2, \omega^7$	$\omega^4, \omega^7, \omega$	$1, \omega, \omega^7$	ω^2	ω, ω^7
$D_1(i)$	$\omega, \omega^5, 1$	$\omega, \omega^6, 1$	$1, \omega^6, \omega^5$	ω^2	ω, ω^7
(ii)	$\omega, 1, \omega^7$	$\omega^7, \omega^4, \omega^2$	$1, \omega^4, \omega^7$	ω^5	1
(iii)	$\omega, \omega^7, \omega^2$	$1, \omega, \omega^3$	$1, \omega^7, \omega^3$	ω^2	ω^7
(iv)	$\omega^5, \omega^2, \omega^7$	$\omega^2, \omega^4, \omega^7$	$1, \omega, \omega^2$	ω^5	1
(v)	$\omega^5, \omega, 1$	$\omega^5, \omega^6, 1$	$1, \omega, \omega^6$	ω^5	1
$D_2(i)$	$\omega, 1, \omega^5$	$\omega, 1, \omega^6$	$1, \omega^5, \omega^6$	ω^2	ω, ω^7
(ii)	$\omega, \omega^7, 1$	$\omega^7, \omega^2, \omega^4$	$1, \omega^4, \omega^7$	ω^5	1
(iii)	$\omega, \omega^2, \omega^7$	$1, \omega^3, \omega$	$1, \omega^7, \omega^3$	ω^2	ω^7
(iv)	$\omega^5, \omega^7, \omega^2$	$\omega^2, \omega^7, \omega^4$	$1, \omega, \omega^2$	ω^5	1
(v)	$\omega^5, 1, \omega$	$\omega^5, 1, \omega^6$	$1, \omega, \omega^6$	ω^5	1
$F_1(i)$	$\omega^3, \omega^7, \omega^2$	$\omega^4, \omega^3, \omega^6$	$1, \omega, \omega^6$	ω^5	ω, ω^2
(ii)	$\omega^3, \omega^2, \omega^7$	$\omega^4, \omega^6, \omega^3$	$1, \omega, \omega^6$	ω^5	ω, ω^2
(iii)	$1, \omega^4, \omega^2$	$\omega^2, \omega^4, \omega$	$1, \omega^6, \omega^5$	ω^3	ω^5, ω
(iv)	$1, \omega^4, \omega^2$	$\omega^2, \omega^4, \omega^3$	$1, \omega^6, \omega^3$	ω^3	ω^5, ω
$F_2(i)$	$\omega^7, \omega^3, \omega^2$	$\omega^3, \omega^4, \omega^6$	$1, \omega^6, \omega$	ω^5	ω, ω^2
(ii)	$\omega^2, \omega^5, \omega$	$\omega^4, \omega^2, \omega^7$	$1, \omega, \omega^2$	ω^5	ω, ω^2
(iii)	$\omega, \omega^3, 1$	$\omega^7, \omega^4, \omega$	$1, \omega, \omega^7$	ω^3	ω^5, ω
(iv)	$\omega^4, \omega^5, \omega^6$	$\omega^4, \omega, \omega^5$	$1, \omega^2, \omega^5$	ω^3	ω^5, ω
$F_3(i)$	$\omega^7, \omega^2, \omega^3$	$\omega^3, \omega^6, \omega^4$	$1, \omega^6, \omega$	ω^5	ω, ω^2
(ii)	$\omega^2, \omega, \omega^5$	$\omega^4, \omega^7, \omega^2$	$1, \omega^2, \omega$	ω^5	ω, ω^2
(iii)	$\omega, 1, \omega^3$	$\omega^7, \omega, \omega^4$	$1, \omega, \omega^7$	ω^7	$1, \omega$
(iv)	$\omega^4, \omega^6, \omega^5$	$\omega^4, \omega^5, \omega$	$1, \omega^2, \omega^5$	ω^7	$1, \omega$

$$\nu_{e_R} \to \omega \nu_{e_R}, \quad \nu_{\mu_R} \to \omega^7 \nu_{\mu_R}, \quad \nu_{\tau_R} \to \omega^5 \nu_{\tau_R}, \quad \chi \to \omega^6 \chi \tag{43}$$

Textures that are realized by the diagonal RH Majorana mass matrix $M_R^{(7)}$, we consider the transformations of ν_{kR}, χ as:

$$\nu_{e_R} \to \nu_{e_R}, \quad \nu_{\mu_R} \to \omega^4 \nu_{\mu_R}, \quad \nu_{\tau_R} \to \omega \nu_{\tau_R}, \quad \chi \to \omega^6 \chi \tag{44}$$

Z_8 transformations of the left-handed $SU(2)_L$ doublets $\bar{D}_{j_L}$, right-handed $SU(2)_L$ singlets l_R, Higgs doublets ϕ, singlet field 'S' and scalar singlets λ of all the basic cases for each texture are presented in Table 13.

7. Conclusion

We have considered the MES (3+1) model of active-sterile neutrino oscillations with one eV mass scale sterile neutrino for resolving the anomalous results of various reactor, radio-chemical and accelerator based neutrino experiments. We have discussed briefly the minimal extended see-saw mechanism that imposes the condition on $M_\nu^{4\times4}$ to be of rank 3 along with both M_D and M_R to be invertible. Then we have undertaken the study of texture zeros of the fermion mass matrices that reduces the complexity of the free parameters and leads to the testable correlations among the elements of neutrino mass matrices. Again texture zeros indicate the underlying symmetry of the models. In our work, we have taken 15 phenomenologically viable two-zero textures of $M_\nu^{4\times4}$ [61] under consideration, of which 12 two-zero textures are found to be of rank 3 for MES realization: A_1, A_2, B_3, B_4, C, D_1, D_2, E_1, E_2, F_1, F_2, F_3. For realization of these two-zero textures, the predictive case i.e., the sum of zeros of M_D and M_R being 8 in the active sector of $M_\nu^{4\times4}$ have been implemented. In this context, we have considered (5+3) and (6+2) predictive cases of zeros in M_D and M_R along with the admissible texture zeros of M_S. In our analysis, we have found that out of 12 viable two-zero textures of rank 3, only 9 textures (A_1, A_2, B_3, B_4, D_1, D_2, F_1, F_2, F_3) could be realized in the (5+3) scheme while none in (6+2) scheme could be succeeded.

In MES realization of 9 two-zero textures in (5+3) scheme, we have obtained some correlations among the elements, m_{ij} of $M_\nu^{4\times4}$. If the scatter plots of the lhs and rhs of each such correlation of a texture against $\sin\theta_{34}$ with current neutrino data have a reasonable overlapping, we have hypothesised them to be viable models. Accordingly m_{ij} have been calculated with 3σ range of the current neutrino oscillation data using formulae given in Appendix. The scatter plots have been drawn under two conditions (i) keeping the Dirac and Majorana CP phases unconstrained $(0 - 360^0)$ and (ii) constraining the CP phases to certain ranges. It has been observed that there are a number of textures whose viabilities get affected when CP phases are constrained to certain ranges, while for a number of textures the phenomenology remains unchanged when CP phases are constrained to different segments of values or even when CP phases are made to be zero. Accordingly we have classified the textures under two categories (i) CP phase dependent textures and (ii) CP phase independent textures.

In our study we have seen that all 9 textures exhibit reasonable overlappings for some ranges of $\sin\theta_{34}$ when CP phases are unconstrained. However, for some selective ranges of CP phases, some textures are not allowed within $\sin\theta_{34} = (0 - 0.4)$. For example, the phenomenology of the texture $B_3(i)$ is represented by the scatter plots for the correlations as shown in Fig. 1 and 2. It has been observed that CP phases play a fair role in determining the viability of the texture. The textures which exhibit similar phenomenology have been presented in Table 9 with their few ranges of CP phases for which the textures become invalid.

In case of the textures like $D_1(iv)$ of which the scatter plots are in (Fig. 3), it has been observed that for unconstrained CP phases, the texture is viable within the complete range of $\sin\theta_{34} = (0-0.4)$, while on constraining the CP phases, the allowed range of $\sin\theta_{34}$ have been squeezed to $(0.06-0.4)$. The texture has been found to be viable at least for some range of $\sin\theta_{34}$ whatever choice of the ranges of the CP phases. Textures showing similar phenomenology have been listed in Table 10 with their respective allowed range of $\sin\theta_{34}$ under unconstrained and constrained CP phases. The constrained ranges of CP phases for each texture have been presented in Table 11.

It has been observed that the textures: $A_2(i)$ and $B_4(iii)$ remain unaffected whether CP phases are unconstrained or constrained to different ranges. On surveying these textures for different segments of the six CP phases, it has been observed that the correlations are allowed for all values of $\sin\theta_{34}$. These textures are insensitive to variation of CP phases and are therefore categorised as CP phase independent textures. As a representative case realization of texture $B_4(iii)$ have been presented in section 5.2. The CP phase independent nature of the texture has been depicted in the scatter plots in Fig. 6 for unconstrained CP phases and Fig. 7 and Fig. 8 for different ranges of constrained CP phases.

For each of the textures, we have calculated the effective neutrino mass $|m_{\beta\beta}|$ for the considered constrained range of Majorana CP phases. For all the textures with respective constrained range of Majorana CP phases, $|m_{\beta\beta}|$ has been found to lie within experimental constraints. In addition, we have also calculated the Jarlskog invariant J_{CP} for each texture with their corresponding constrained ranges of Dirac CP phases. In the (3+1) scheme, we have observed that, $J_{CP} \neq 0$ for $\delta_{13} = 0$ which differs from the case of three neutrino scenario.

Also, it has been observed that there exist S_3 transformations of a given combination of M_D, M_R, M_S leading to a particular two-zero textures of $M_\nu^{4\times4}$ which give the same correlations. This enables us to study only few basic combinations of M_D, M_R and M_S instead of all possible five-zero textures of M_D and three-zero textures of M_R. As a representative case Table 5 shows the combinations of M_D, M_R and M_S which are obtained via S_3 transformation from the basic combination in Eq. (18) for texture $B_3(i)$. Basic combinations of each of the textures have been listed in Table 8.

The viable textures have been finally realized by means of Z_8 Abelian flavor symmetry group. With the charged lepton mass matrix M_l as diagonal and with 5 zeros in M_D we have required three Higgs doublet Φ_1, Φ_2, Φ_3, one of which is the SM Higgs (Φ_1) which transforms trivially under Z_8. To realize the three-zero texture of M_R, one scalar singlet χ is required. For one-zero texture of M_S, two additional scalar singlets (λ_1, λ_2) are needed, while one singlet λ_1 for the two-zero texture of M_S. Also, we have considered Z_8 transformation of the singlet chiral field 'S', in order to prevent bare mass term of 'S' as demanded by MES mechanism. We have presented the symmetry realization of texture $B_3(i)$ as a representative case. We have also demonstrated the symmetry realization of the Case (b) (Table 5) to show that all the S_3 symmetric textures also follow S_3 transformations of the fields of the basic combinations.

In this work we have succeeded to obtain viable two-zero textures of (3+1) MES neutrino mass matrices M_ν in (5+3) predictive scheme of M_D and M_R, and one/two zero in M_S and their Z_8 symmetry realization. There are further scope for study of these textures from other aspects like unstable sterile state i.e., (3+1+decay) model.

Declaration of competing interest

The authors declare that they have no known competing financial interests or personal relationships that could have appeared to influence the work reported in this paper.

Appendix A. Light neutrino mass matrix elements

$$m_{ee} = c_{12}^2 c_{13}^2 c_{14}^2 m_1 + e^{-i\alpha} c_{13}^2 c_{14}^2 m_2 s_{12}^2 + e^{-i\beta} c_{14}^2 m_3 s_{13}^2 + e^{-i\gamma} m_4 s_{14}^2, \tag{45}$$

$$\begin{aligned} m_{e\mu} = {} & e^{i(\delta-14-\delta_{24}-\gamma)} c_{14} m_4 s_{14} s_{24} + c_{12} c_{13} c_{14} m_1 (-c_{23} c_{24} s_{12} - e^{i\delta_{13}} c_{12} c_{24} s_{13} s_{23} \\ & - e^{i(\delta_{14}-\delta_{24})} c_{12} c_{13} s_{14} s_{24}) + e^{-i\alpha} c_{13} c_{14} m_2 s_{12} (c_{12} c_{23} c_{24} - e^{i\delta_{13}} c_{24} s_{12} s_{13} s_{23} \\ & - e^{i(\delta_{14}-\delta_{24})} c_{13} s_{12} s_{14} s_{24}) + e^{-i(\beta+\delta_{24})} c_{14} m_3 s_{13} (e^{i(\delta_{13}+\delta_{24})} c_{13} c_{24} s_{23} \\ & - e^{i\delta_{14}} s_{13} s_{14} s_{24})), \end{aligned} \tag{46}$$

$$\begin{aligned} m_{e\tau} = {} & e^{-\frac{i\gamma}{2} - \frac{1}{2} i(\gamma - 2\delta_{14})} c_{14} c_{24} m_4 s_{14} s_{34} + c_{12} c_{13} c_{14} m_1 (-e^{i\delta_{13}} c_{12} c_{23} c_{34} s_{13} + c_{34} s_{12} s_{23} \\ & - e^{i\delta_{14}} c_{12} c_{13} c_{24} s_{14} s_{34} + e^{i\delta_{24}} (c_{23} s_{12} + e^{i\delta_{13}} c_{12} s_{13} s_{23}) s_{24} s_{34}) \\ & - e^{-i\alpha} c_{13} c_{14} m_2 s_{12} (e^{i\delta_{13}} c_{23} c_{34} s_{12} s_{13} + c_{12} c_{34} s_{23} \\ & + e^{i\delta_{14}} c_{13} c_{24} s_{12} s_{14} s_{34} + e^{i\delta_{24}} (c_{12} c_{23} - e^{i\delta_{13}} s_{12} s_{13} s_{23}) s_{24} s_{34}) + e^{-i\beta} c_{14} m_3 s_{13} \\ & \times (-e^{i\delta_{14}} c_{24} s_{13} s_{14} s_{34} + e^{i\delta_{13}} c_{13} (c_{23} c_{34} - e^{i\delta_{24}} s_{23} s_{24} s_{34})), \end{aligned} \tag{47}$$

$$\begin{aligned} m_{es} = {} & e^{-\frac{i\gamma}{2} - \frac{1}{2} i(\gamma - 2\delta_{14})} c_{14} c_{24} c_{34} m_4 s_{14} + e^{-i\beta} c_{14} m_3 s_{13} (-e^{i\delta_{14}} c_{24} c_{34} s_{13} s_{14} \\ & - e^{i\delta_{13}} c_{13} (e^{i\delta_{24}} c_{34} s_{23} s_{24} + c_{23} s_{34})) + c_{12} c_{13} c_{14} m_1 (-e^{i\delta_{14}} c_{12} c_{13} c_{24} c_{34} s_{14} \\ & + e^{i\delta_{24}} c_{23} c_{34} s_{12} s_{24} - s_{12} s_{23} s_{34} + e^{i\delta_{13}} c_{12} s_{13} (e^{i\delta_{24}} c_{34} s_{23} s_{24} + c_{23} s_{34})) \\ & + e^{-i\alpha} c_{13} c_{14} m_2 s_{12} (-e^{i\delta_{14}} c_{13} c_{24} c_{34} s_{12} s_{14} - e^{i\delta_{24}} c_{12} c_{23} c_{34} s_{24} \\ & + c_{12} s_{23} s_{34} + e^{i\delta_{13}} s_{12} s_{13} (e^{i\delta_{24}} c_{34} s_{23} s_{24} + c_{23} s_{34})), \end{aligned} \tag{48}$$

$$\begin{aligned} m_{\mu\mu} = {} & e^{-i(\gamma - 2\delta_{14} + 2\delta_{24})} c_{14}^2 m_4 s_{24}^2 + m_1 (-c_{23} c_{24} s_{12} - e^{i\delta_{13}} c_{12} c_{24} s_{13} s_{23} \\ & - e^{i(\delta_{14}-\delta_{24})} c_{12} c_{13} s_{14} s_{24})^2 + e^{-i\alpha} m_2 (c_{12} c_{23} c_{24} - e^{i\delta_{13}} c_{24} s_{12} s_{13} s_{23} \\ & - e^{i(\delta_{14}-\delta_{24})} c_{13} s_{12} s_{14} s_{24})^2 + e^{-i(\beta+2\delta_{24})} m_3 (e^{i(\delta_{13}+\delta_{24})} c_{13} c_{24} s_{23} \\ & - e^{i\delta_{14}} s_{13} s_{14} s_{24})^2), \end{aligned} \tag{49}$$

$$\begin{aligned} m_{\mu\tau} = {} & e^{-\frac{1}{2} i(\gamma - 2\delta_{14}) - \frac{1}{2} i(\gamma - 2\delta_{14} + 2\delta_{24})} c_{14}^2 c_{24} m_4 s_{24} s_{34} + m_1 (-c_{23} c_{24} s_{12} - e^{i\delta_{13}} c_{12} c_{24} s_{13} s_{23} \\ & - e^{i(\delta_{14}-\delta_{24})} c_{12} c_{13} s_{14} s_{24}) (-e^{i\delta_{13}} c_{12} c_{23} c_{34} s_{13} + c_{34} s_{12} s_{23} - e^{i\delta_{14}} c_{12} c_{13} c_{24} s_{14} s_{34} \\ & + e^{i\delta_{24}} (c_{23} s_{12} + e^{i\delta_{13}} c_{12} s_{13} s_{23}) s_{24} s_{34}) - e^{-i\alpha} m_2 (c_{12} c_{23} c_{24} - e^{i\delta_{13}} c_{24} s_{12} s_{13} s_{23} - e^{i(\delta_{14}-\delta_{24})} \\ & c_{13} s_{12} s_{14} s_{24}) (e^{i\delta_{13}} c_{23} c_{34} s_{12} s_{13} + c_{12} c_{34} s_{23} + e^{i\delta_{14}} c_{13} c_{24} s_{12} s_{14} s_{34} + e^{i\delta_{24}} (c_{12} c_{23} \\ & - e^{i\delta_{13}} s_{12} s_{13} s_{23}) s_{24} s_{34}) + e^{-\frac{i\beta}{2} - \frac{1}{2} i(\beta + 2\delta_{24})} m_3 (e^{i(\delta_{13}+\delta_{24})} c_{13} c_{24} s_{23} - e^{i\delta_{14}} s_{13} s_{14} s_{24}) \\ & (-e^{i\delta_{14}} c_{24} s_{13} s_{14} s_{34} + e^{i\delta_{13}} c_{13} (c_{23} c_{34} - e^{i\delta_{24}} s_{23} s_{24} s_{34})), \end{aligned} \tag{50}$$

$$\begin{aligned} m_{\mu s} = {} & e^{-\frac{1}{2} i(\gamma - 2\delta_{14}) - \frac{1}{2} i(\gamma - 2\delta_{14} + 2\delta_{24})} c_{14}^2 c_{24} c_{34} m_4 s_{24} + e^{-\frac{i\beta}{2} - \frac{1}{2} i(\beta + 2\delta_{24})} m_3 (e^{i(\delta_{13}+\delta_{24})} \\ & c_{13} c_{24} s_{23} - e^{i\delta_{14}} s_{13} s_{14} s_{24}) (-e^{i\delta_{14}} c_{24} c_{34} s_{13} s_{14} - e^{i\delta_{13}} c_{13} (e^{i\delta_{24}} c_{34} s_{23} s_{24} + c_{23} s_{34})) + \\ & m_1 (-c_{23} c_{24} s_{12} - e^{i\delta_{13}} c_{12} c_{24} s_{13} s_{23} - e^{i(\delta_{14}-\delta_{24})} c_{12} c_{13} s_{14} s_{24}) (-e^{i\delta_{14}} c_{12} c_{13} c_{24} c_{34} s_{14} \\ & + e^{i\delta_{24}} c_{23} c_{34} s_{12} s_{24} - s_{12} s_{23} s_{34} + e^{i\delta_{13}} c_{12} s_{13} (e^{i\delta_{24}} c_{34} s_{23} s_{24} + c_{23} s_{34})) + \\ & e^{-i\alpha} m_2 (c_{12} c_{23} c_{24} - e^{i\delta_{13}} c_{24} s_{12} s_{13} s_{23} - e^{i(\delta_{14}-\delta_{24})} c_{13} s_{12} s_{14} s_{24}) (-e^{i\delta_{14}} c_{13} c_{24} c_{34} s_{12} s_{14} \\ & - e^{i\delta_{24}} c_{12} c_{23} c_{34} s_{24} + c_{12} s_{23} s_{34} + e^{i\delta_{13}} s_{12} s_{13} (e^{i\delta_{24}} c_{34} s_{23} s_{24} + c_{23} s_{34})), \end{aligned} \tag{51}$$

$$m_{\tau\tau} = e^{-i(\gamma-2\delta_{14})}c_{14}^2c_{24}^2m_4s_{34}^2 + m_1(-e^{i\delta_{13}}c_{12}c_{23}c_{34}s_{13} + c_{34}s_{12}s_{23} - e^{i\delta_{14}}c_{12}c_{13}c_{24}s_{14}s_{34} + e^{i\delta_{24}}(c_{23}s_{12} + e^{i\delta_{13}}c_{12}s_{13}s_{23})s_{24}s_{34})^2 + e^{-i\alpha}m_2(e^{i\delta_{13}}c_{23}c_{34}s_{12}s_{13} + c_{12}c_{34}s_{23} + e^{i\delta_{14}}c_{13}c_{24}s_{12}s_{14}s_{34} + e^{i\delta_{24}}(c_{12}c_{23} - e^{i\delta_{13}}s_{12}s_{13}s_{23})s_{24}s_{34})^2 + e^{-i\beta}m_3 (-e^{i\delta_{14}}c_{24}s_{13}s_{14}s_{34} + e^{i\delta_{13}}c_{13}(c_{23}c_{34} - e^{i\delta_{24}}s_{23}s_{24}s_{34}))^2, \quad (52)$$

$$m_{\tau s} = e^{-i(\gamma-2\delta_{14})}c_{14}^2c_{24}^2c_{34}m_4s_{34} + m_1(-e^{i\delta_{13}}c_{12}c_{23}c_{34}s_{13} + c_{34}s_{12}s_{23} - e^{i\delta_{14}}c_{12}c_{13}c_{24}s_{14}s_{34} + e^{i\delta_{24}}(c_{23}s_{12} + e^{i\delta_{13}}c_{12}s_{13}s_{23})s_{24}s_{34})(-e^{i\delta_{14}}c_{12}c_{13}c_{24}c_{34}s_{14} + e^{i\delta_{24}}c_{23}c_{34}s_{12}s_{24} - s_{12}s_{23}s_{34} + e^{i\delta_{13}}c_{12}s_{13}(e^{i\delta_{24}}c_{34}s_{23}s_{24} + c_{23}s_{34})) - e^{-i\alpha}m_2(e^{i\delta_{13}}c_{23}c_{34}s_{12}s_{13} + c_{12}c_{34}s_{23} + e^{i\delta_{14}}c_{13}c_{24}s_{12}s_{14}s_{34} + e^{i\delta_{24}}(c_{12}c_{23} - e^{i\delta_{13}}s_{12}s_{13}s_{23})s_{24}s_{34})(-e^{i\delta_{14}}c_{13}c_{24}c_{34}s_{12}s_{14} - e^{i\delta_{24}}c_{12}c_{23}c_{34}s_{24} + c_{12}s_{23}s_{34} + e^{i\delta_{13}}s_{12}s_{13}(e^{i\delta_{24}}c_{34}s_{23}s_{24} + c_{23}s_{34})) + e^{-i\beta}m_3(-e^{i\delta_{14}}c_{24}c_{34}s_{13}s_{14} - e^{i\delta_{13}}c_{13}(e^{i\delta_{24}}c_{34}s_{23}s_{24} + c_{23}s_{34}))(-e^{i\delta_{14}}c_{24}s_{13}s_{14}s_{34} + e^{i\delta_{13}}c_{13}(c_{23}c_{34} - e^{i\delta_{24}}s_{23}s_{24}s_{34})), \quad (53)$$

$$m_{ss} = e^{-i(\gamma-2\delta_{14})}c_{14}^2c_{24}^2c_{34}^2m_4 + e^{-i\beta}m_3(-e^{i\delta_{14}}c_{24}c_{34}s_{13}s_{14} - e^{i\delta_{13}}c_{13}(e^{i\delta_{24}}c_{34}s_{23}s_{24} + c_{23}s_{34}))^2 + m_1(-e^{i\delta_{14}}c_{12}c_{13}c_{24}c_{34}s_{14} + e^{i\delta_{24}}c_{23}c_{34}s_{12}s_{24} - s_{12}s_{23}s_{34} + e^{i\delta_{13}}c_{12}s_{13}(e^{i\delta_{24}}c_{34}s_{23}s_{24} + c_{23}s_{34}))^2 + e^{-i\alpha}m_2(-e^{i\delta_{14}}c_{13}c_{24}c_{34}s_{12}s_{14} - e^{i\delta_{24}}c_{12}c_{23}c_{34}s_{24} + c_{12}s_{23}s_{34} + e^{i\delta_{13}}s_{12}s_{13}(e^{i\delta_{24}}c_{34}s_{23}s_{24} + c_{23}s_{34}))^2. \quad (54)$$

References

[1] Z.-z. Xing, Flavor structures of charged fermions and massive neutrinos, Phys. Rep. 854 (2020), arXiv:1909.09610 [hep-ph].
[2] S. Boser, et al., Status of light sterile neutrino searches, Prog. Part. Nucl. Phys. 111 (2020) 103736, arXiv:1906.01739.
[3] C. Athanassopoulos, et al., LSND Collaboration, Candidate events in a search for $\bar{\nu}_\mu \to \bar{\nu}_e$ oscillations, Phys. Rev. Lett. 75 (1995) 2650–2653, arXiv:nucl-ex/9504002.
[4] A. Bazarko, MiniBooNE: status of the booster neutrino experiment, Nucl. Phys. Proc. Suppl. 91 (2001) 210–215, arXiv:hep-ex/0009056.
[5] W. Hampel, et al., GALLEX solar neutrino observations: results for GALLEX IV, Phys. Lett. B 447 (1999) 127–133.
[6] J.N. Abdurashitov, et al., Measurement of the solar neutrino capture rate with gallium metal, Phys. Rev. C 60 (1999) 055801, arXiv:astro-ph/9907113.
[7] J. Kostensalo, J. Suhonen, C. Giunti, P.C. Srivastava, The gallium anomaly revisited, Phys. Lett. B 795 (2019) 542–547, arXiv:1906.10980.
[8] T.A. Mueller, et al., Improved predictions of reactor antineutrino spectra, Phys. Rev. C 83 (2011) 054615, arXiv:1101.2663.
[9] P. Huber, On the determination of anti-neutrino spectra from nuclear reactors, Phys. Rev. C 84 (2011) 024617, Erratum: Phys. Rev. C 85 (2012) 029901, arXiv:1106.0687.
[10] F.P. An, et al., Evolution of the reactor antineutrino flux and spectrum at Daya Bay, Phys. Rev. Lett. 118 (25) (2017) 251801, arXiv:1704.01082.
[11] Y.J. Ko, et al., Sterile neutrino search at the NEOS experiment, Phys. Rev. Lett. 118 (12) (2017) 121802, arXiv:1610.05134.
[12] I. Alekseev, et al., Search for sterile neutrinos at the DANSS experiment, Phys. Lett. B 787 (2018) 56–63, arXiv:1804.04046.
[13] H. Almazn, et al., Sterile neutrino constraints from the STEREO experiment with 66 days of reactor-on data, Phys. Rev. Lett. 121 (16) (2018) 161801, arXiv:1806.02096.

[14] J. Ashenfelter, et al., Measurement of the antineutrino spectrum from 235 U fission at HFIR with PROSPECT, Phys. Rev. Lett. 122 (25) (2019) 251801, arXiv:1812.10877.
[15] A.P. Serebrov, et al., First observation of the oscillation effect in the Neutrino-4 experiment on the search for the sterile neutrino, Pis'ma Zh. Eksp. Teor. Fiz. 109 (4) (2019) 209–218, JETP Lett. 109 (4) (2019) 213, arXiv:1809.10561.
[16] Y. Abreu, et al., Performance of a full scale prototype detector at the BR2 reactor for the SoLid experiment, J. Instrum. 13 (05) (2018) P05005, arXiv:1802.02884.
[17] J. Barry, W. Rodejohann, H. Zhang, Light sterile neutrinos: models and phenomenology, J. High Energy Phys. 1107 (2011) 091, arXiv:1105.3911.
[18] N. Aghanim, et al., Planck 2018 results. VI. Cosmological parameters, arXiv:1807.06209.
[19] P.A.R. Ade, et al., Planck Collaboration, Planck 2015 results. XIII. Cosmological parameters, Astron. Astrophys. 594 (2016) A13, arXiv:1502.01589 [astro-ph.CO].
[20] S. Joudaki, K.N. Abazajian, M. Kaplinghat, Are light sterile neutrinos preferred or disfavored by cosmology?, Phys. Rev. D 87 (2013) 065003.
[21] T.D. Jacques, L.M. Krauss, C. Lunardini, Additional light sterile neutrinos and cosmology, Phys. Rev. D 87 (2013) 083515, Erratum: Phys. Rev. D 88 (2013) 109901.
[22] A. Mirizzi, et al., The strongest bounds on active-sterile neutrino mixing after Planck data, Phys. Lett. B 726 (2013) 8.
[23] M. Maltoni, et al., Constraining neutrino oscillation parameters with current solar and atmospheric data, Phys. Rev. D 67 (2003) 013011, arXiv:hep-ph/0207227.
[24] A. Diaz, et al., Where are we with light sterile neutrinos, arXiv:1906.00045.
[25] C. Giunti, M. Laveder, 3+1 and 3+2 sterile neutrino fits, Phys. Rev. D 84 (2011) 073008, arXiv:1107.1452.
[26] J.J. Gomez-Cadenas, M.C. Gonzalez-Garcia, Future ν_τ oscillation experiments and present data, Z. Phys. C 71 (1996) 443, arXiv:hep-ph/9504246.
[27] S. Goswami, Accelerator, reactor, solar and atmospheric neutrino oscillation: beyond three generations, Phys. Rev. D 55 (1997) 2931–2949.
[28] N. Okada, O. Yasuda, A sterile neutrino scenario constrained by experiments and cosmology, Int. J. Mod. Phys. A 12 (1997) 3669–3694.
[29] V.D. Barger, T.J. Weiler, K. Whisnant, Four-way neutrino oscillations, Phys. Lett. B 427 (1998) 97, arXiv:hep-ph/9712495.
[30] G. Mention, et al., The reactor antineutrino anomaly, Phys. Rev. D 83 (2011) 073006, arXiv:1101.2755.
[31] F. An, et al., Neutrino physics with JUNO, J. Phys. G 43 (3) (2016) 030401, arXiv:1507.05613;
Z.-Z. Xing, Interference effects in reactor antineutrino oscillations, arXiv:1808.02256.
[32] P. Adamson, et al., Limits on active to sterile neutrino oscillations from disappearance searches in the MINOS, Daya Bay, and Bugey-3 experiments, Phys. Rev. Lett. 117 (15) (2016) 151801, Addendum: Phys. Rev. Lett. 117 (20) (2016) 209901, arXiv:1607.01177.
[33] Y.-F. Li, S. Luo, Neutrino oscillation probabilities in matter with direct and indirect unitarity violation in the lepton mixing matrix, Phys. Rev. D 93 (3) (2016) 033008, arXiv:1508.00052.
[34] J. Tang, Y. Zhang, Y.-F. Li, Probing direct and indirect unitarity violation in future accelerator neutrino facilities, Phys. Lett. B 774 (2017) 217–224, arXiv:1708.04909.
[35] H. Zhang, Light sterile neutrino in the minimal extended seesaw, Phys. Lett. B 714 (2012) 262–266, arXiv:1110.6838.
[36] J. Heeck, H. Zhang, Exotic charges, multicomponent dark matter and light sterile neutrinos, J. High Energy Phys. 05 (2013) 164, arXiv:1211.0538.
[37] S. Weinberg, The problem of mass, Trans. N. Y. Acad. Sci. 38 (1977) 185–201.
[38] F. Wilczek, A. Zee, Discrete flavor symmetries and a formula for the Cabibbo angle, Phys. Lett. B 70 (1977) 418, Erratum: Phys. Lett. B 72 (1978) 504.
[39] H. Fritzsch, Calculating the Cabibbo angle, Phys. Lett. B 70 (1977) 436–440.
[40] H. Fritzsch, Weak interaction mixing in the six-quark theory, Phys. Lett. B 73 (1978) 317–322.
[41] H. Fritzsch, Quark masses and flavor mixing, Nucl. Phys. B 155 (1979) 189–207.
[42] G.C. Branco, D. Emmanuel-Costa, M.N. Rebelo, P. Roy, Four zero neutrino Yukawa textures in the minimal seesaw framework, Phys. Rev. D 77 (2008) 053011, arXiv:0712.0774.
[43] S. Goswami, A. Watanabe, Minimal seesaw textures with two heavy neutrinos, Phys. Rev. D 79 (2009) 033004, arXiv:0807.3438.
[44] S. Goswami, S. Khan, A. Watanabe, Hybrid textures in minimal seesaw mass matrices, Phys. Lett. B 693 (2010) 249–254, arXiv:0811.4744.

[45] S. Choubey, W. Rodejohann, P. Roy, Phenomenological consequences of four zero neutrino Yukawa textures, Nucl. Phys. B 808 (2009) 272–291, arXiv:0807.4289, Erratum: Nucl. Phys. B 818 (2009) 136.
[46] L. Lavoura, New texture-zero patterns for lepton mixing, J. Phys. G 42 (2015) 105004, arXiv:1502.0300.
[47] W. Grimus, A.S. Joshipura, L. Lavoura, M. Tanimoto, Symmetry realization of texture zeros, Eur. Phys. J. C 36 (2004) 227–232, arXiv:hep-ph/0405016.
[48] Walter Grimus, Neutrino mass matrices, texture zeros and family symmetries, arXiv:hep-ph/0511078, 2005.
[49] W. Grimus, P. Ludl, Two-parameter neutrino mass matrices with two texture zeros, J. Phys. G 40 (2013) 055003, arXiv:1208.4515.
[50] H. Fritzsch, Z.-z. Xing, S. Zhou, Two-zero textures of the Majorana neutrino mass matrix and current experimental tests, J. High Energy Phys. 1109 (2011) 083, arXiv:1108.4534.
[51] D. Meloni, G. Blankenburg, Fine-tuning and naturalness issues in the two-zero neutrino mass textures, Nucl. Phys. B 867 (2013) 749–762, arXiv:1204.2706.
[52] P. Ludl, S. Morisi, E. Peinado, The reactor mixing angle and CP violation with two texture zeros in the light of T2K, Nucl. Phys. B 857 (2012) 411–423, arXiv:1109.3393.
[53] S. Dev, S. Kumar, S. Verma, S. Gupta, Phenomenology of two-texture zero neutrino mass matrices, Phys. Rev. D 76 (2007) 013002, arXiv:hep-ph/0612102.
[54] Z.-z. Xing, Texture zeros and Majorana phases of the neutrino mass matrix, Phys. Lett. B 530 (2002) 159–166, arXiv:hep-ph/0201151.
[55] Z.-z. Xing, A full determination of the neutrino mass spectrum from two zero textures of the neutrino mass matrix, Phys. Lett. B 539 (2002) 85–90, arXiv:hep-ph/0205032.
[56] B.R. Desai, D. Roy, A.R. Vaucher, Three neutrino mass matrices with two texture zeros, Mod. Phys. Lett. A 18 (2003) 1355–1366, arXiv:hep-ph/0209035.
[57] S. Dev, S. Kumar, S. Verma, S. Gupta, CP violation in two texture zero neutrino mass matrices, Phys. Lett. B 656 (2007) 79–82, arXiv:0708.3321.
[58] R.R. Gautam, M. Singh, M. Gupta, Neutrino mass matrices with one texture zero and a vanishing neutrino mass, Phys. Rev. D 92 (2015) 013006, arXiv:1506.0486.
[59] S. Dev, S. Kumar, S. Verma, S. Gupta, Phenomenological implications of a class of neutrino mass matrices, Nucl. Phys. B 784 (2007) 103–117, arXiv:hep-ph/0611313.
[60] S. Kumar, Implications of a class of neutrino mass matrices with texture zeros for non-zero, θ_{13}, Phys. Rev. D 84 (2011) 077301, arXiv:1108.2137.
[61] M. Ghosh, S. Goswami, S. Gupta, Two zero mass matrices and sterile neutrinos, J. High Energy Phys. 04 (2013) 103, arXiv:1211.0118 [hep-ph].
[62] Y. Zhang, Majorana neutrino mass matrices with three texture zeros and the sterile neutrino, Phys. Rev. D 87 (2013) 053020, arXiv:1301.7302.
[63] D. Borah, M. Ghosh, S. Gupta, S. Prakash, S.K. Raut, Analysis of four-zero textures in the 3+1 neutrino framework, Phys. Rev. D 94 (2016) 113001, arXiv:1606.02076.
[64] P.H. Frampton, S.L. Glashow, D. Marfatia, Zeroes of the neutrino mass matrix, Phys. Lett. B 536 (2002) 79, arXiv:hep-ph/0201008.
[65] M. Patgiri, P. Kumar, D. Sarma, Study of texture zeros of fermion mass matrices in minimal extended seesaw mechanism and symmetry realization, Int. J. Mod. Phys. A 32 (27) (2017) 1750168.
[66] N. Nath, M. Ghosh, S. Goswami, S. Gupta, J. High Energy Phys. 03 (2017) 075, arXiv:1610.09090.
[67] M. Patgiri, P. Kumar, Understanding of two-zero textures of neutrino mass matrices in minimal extended seesaw mechanism and their symmetry realization, Int. J. Mod. Phys. A 34 (11) (2019) 1950059.
[68] S. Goswami, W. Rodejohann, Constraining mass spectra with sterile neutrinos from neutrinoless double beta decay, tritium beta decay and cosmology, Phys. Rev. D 73 (2006) 113003, arXiv:hep-ph/0512234.
[69] F. Capozzi, E. Lisi, A. Marrone, D. Montanino, A. Palazzo, Neutrino masses and mixings: status of known and unknown 3ν parameters, Nucl. Phys. B 908 (2016) 218–234, arXiv:1601.07777.
[70] S. Gariazzo, C. Giunti, M. Laveder, Y.F. Li, E.M. Zavanin, Light sterile neutrinos, J. Phys. G 43 (2016) 033001, arXiv:1507.0820.
[71] C. Giunti, Oscillations beyond three-neutrino mixing, talk given at Proceedings of Neutrino 2016, London, UK, 2016.
[72] T. Schwetz, Global oscillation fits with sterile neutrinos, talk given at Proceedings of Sterile Neutrino Crossroads, 2011, Virginia Tech, USA, 2011.
[73] D.R. Artusa, et al., CUORE, Searching for neutrinoless double-beta decay of ^{130}Te with CUORE, Adv. High Energy Phys. 2015 (2015) 879871, arXiv:1402.6072 [physics.ins-det].
[74] M. Agostini, et al., GERDA, Improved limit on neutrinoless double beta decay of ^{76}Ge from GERDA phase II, Phys. Rev. Lett. 120 (2018) 132503, arXiv:1803.11100 [nucl-ex].

[75] M. Auger, et al., Search for neutrinoless double-beta decay in with EXO-200, Phys. Rev. Lett. 109 (2012) 032505, arXiv:1205.5608.
[76] A. Gando, et al., KamLAND-Zen Collaboration, Search for Majorana neutrinos near the inverted mass hierarchy region with KamLAND-Zen, Phys. Rev. Lett. 117 (2016) 082503, arXiv:1605.02889 [hep-ex].